HHS Public Access

Author manuscript

Cell Rep. Author manuscript; available in PMC 2022 August 09.

Published in final edited form as:

Cell Rep. 2022 July 19; 40(3): 111097. doi:10.1016/j.celrep.2022.111097.

Neuropilin-2 axis in regulating secretory phenotype of neuroendocrine-like prostate cancer cells and its implication in therapy resistance

Ridwan Islam[1], **Juhi Mishra**[1,4], **Navatha Shree Polavaram**[1,4], **Sreyashi Bhattacharya**[1], **Zhengdong Hong**[1], **Sanika Bodas**[1], **Sunandini Sharma**[1], **Alyssa Bouska**[1], **Tyler Gilbreath**[1], **Ahmed M. Said**[2], **Lynette M. Smith**[1], **Benjamin A. Teply**[1], **Michael H. Muders**[3], **Surinder K. Batra**[1], **Kaustubh Datta**[1,*], **Samikshan Dutta**[1,5,*]

[1]Department of Biochemistry and Molecular Biology, University of Nebraska Medical Center, BCC, Omaha, NE 68198, USA

[2]Department of Pharmaceutical Organic Chemistry, Faculty of Pharmacy, Helwan University, Ein-Helwan, Helwan, Cairo, Egypt

[3]Department of Prostate Cancer Research, Center for Pathology, University of Bonn Medical Center, Bonn, Germany

[4]These authors contributed equally

[5]Lead contact

SUMMARY

Neuroendocrine (NE)-like tumors secrete various signaling molecules to establish paracrine communication within the tumor milieu and to create a therapy-resistant environment. It is important to identify molecular mediators that regulate this secretory phenotype in NE-like cancer. The current study highlights the importance of a cell surface molecule, Neuropilin-2 (NRP2), for the secretory function of NE-like prostate cancer (PCa). Our analysis on different patient cohorts suggests that NRP2 is high in NE-like PCa. We have developed cell line models to investigate NRP2's role in NE-like PCa. Our bioinformatics, mass spectrometry, cytokine array, and other supporting experiments reveal that NRP2 regulates robust secretory phenotype in NE-like PCa and controls the secretion of factors promoting cancer cell survival. Depletion of NRP2 reduces the secretion of these factors and makes resistant cancer cells sensitive to chemotherapy *in vitro* and

*Correspondence: kaustubh.datta@unmc.edu (K.D.), samikshan.dutta@unmc.edu (S.D.).

AUTHOR CONTRIBUTIONS

R.I. contributed to designing the project and performed most of the work. N.S.P. developed the cell lines, J.M. contributed to Figures 5 though 7 and performed cytokine assay. Z.H., S. Bhattacharya, S. Bodas, and T.G. assisted some of the work. S.S. and A.B. did the bio-informatic analysis. A.M.S. did the mass spectronomy analysis. L.M.S. supervised the statistical analysis. B.A.T. and S.K.B. supervised the study. M.H.M. evaluated IHC images. S.D. and K.D. designed and wrote the project.

DECLARATION OF INTERESTS

The authors declare no competing interests.

SUPPLEMENTAL INFORMATION

Supplemental information can be found online at https://doi.org/10.1016/j.celrep.2022.111097.

in vivo. Therefore, targeting NRP2 can revert cellular secretion and sensitize PCa cells toward therapy.

Graphical abstract

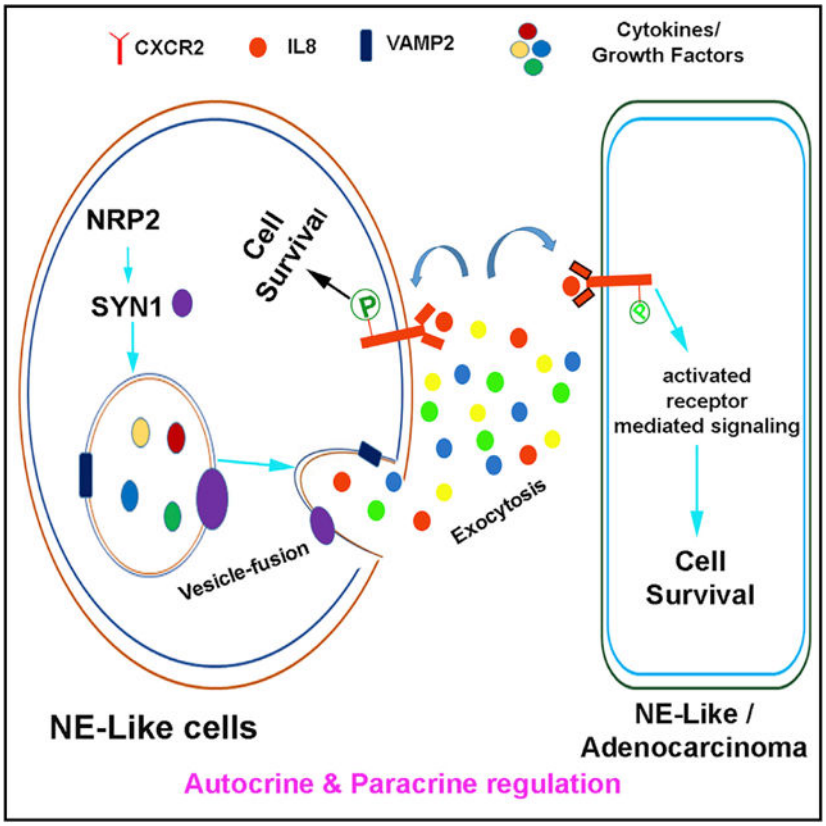

In brief

Islam et al. observe high expression of a cell surface receptor, neuropilin-2 (NRP2), in neuroendocrine-like prostate cancer. NRP2 regulates the secretion of cytokines by facilitating the fusion of secretory vesicles to cell membrane. The secretory products protect not only the neuroendocrine cells but also the adjacent adenocarcinoma from chemotherapies.

INTRODUCTION

Lineage plasticity leading to androgen receptor (AR)-independent prostate cancer (PCa) has gained prominence recently and is being studied as one of the underlying reasons for resistance to second-generation AR inhibitors (ARIs) (Aggarwal et al., 2018; Beltran et al., 2016; Butler and Huang, 2021). Lineage plasticity can be defined as the ability of a cell to change itself into a new phenotype, allowing the cancer cells to survive in a harsh environment such as hypoxia or nutrient deprivation, and is responsible for intratumoral heterogeneity (Beltran et al., 2016; Ku et al., 2017; Mu et al., 2017). Plasticity-driven intratumoral heterogeneity has been attributed as a major reason for acquired resistance to therapy in PCa (Jolly et al., 2018). One of the major histologic subtypes, which appears

due to the oncogenic and therapy-induced plasticity of PCa cells, is the transformation from adenocarcinoma to high-grade neuroendocrine (NE)-like tumors (Aggarwal et al., 2018; Beltran et al., 2016; Butler and Huang, 2021; Tritschler et al., 2017). Therefore, the co-existence of adenocarcinoma (AR-high/NE-marker low) and NE-like (AR-low/NE-marker high) tumor cells is often observed in treatment-resistant aggressive PCa (Quintanal-Villalonga et al., 2020; Li et al., 2019). These NE-like PCa cells do not depend on AR-transcriptional activity for their growth and survival (Mu et al., 2017) and are thus resistant to ARIs. About 25% of the aggressive metastatic castration-resistant PCa (mCRPC) patients develop such treatment-induced NE prostatic adenocarcinoma (t-NEPC) or NE-like PCa (Tritschler et al., 2017; Aparicio et al., 2011). The number of diagnosed t-NEPC cases in PCa patients has been increasing with the advancement of our understanding on the NE-like phenotype (Conteduca et al., 2019). Additionally, patients with NE-like PCa show poor prognosis owing to the heterogeneous feature of the tumors as well as unavailability of effective therapy against this type of cancer (Beltran et al., 2016; Akamatsu et al., 2018). Therefore, lucid understanding on the molecular mechanism of therapy resistance in NE-like PCa and identification of potential molecular targets for developing an effective therapeutic strategy are required.

NE-like cells morphologically display long dendritic processes (Sang et al., 2016) and contain a wide array of dense-core secretory granules (Rindi and Wiedenmann, 2020). The genes that are upregulated during NE-like transdifferentiation include neuronal transcription factors, membrane ion channels, receptors, and secreted biogenic amines, peptides, and cytokines. Neurosecretory peptides like bombesin, gastrin, neuron-specific enolase, parathyroid hormone-related peptide (PTHrP), and cytokines such as interleukin (IL-8) and vascular endothelial growth factor (VEGF) have been reported to act both in an autocrine and paracrine manner to stimulate growth and survival of both the NE-like cancer cells and the surrounding adenocarcinoma (Rindi and Wiedenmann, 2020; Cives et al., 2019; Somasundaram and Taraska, 2018; Zhang et al., 2018; Jin et al., 2004). These secretory factors influence the tumor microenvironment by promoting angiogenesis and anti-tumor immune responses and therefore induce cancer progression (Wright et al., 2003; Zhang et al., 2018). Blocking such pathways is important not only to sensitize the NE-like colonies to therapy but also to reprogram the microenvironment toward more favorable prognosis of the disease. However, a lack of comprehensive understanding of the mechanism for the secretory pathways limits its clinical implication. Therefore, it is important to study the molecular mechanisms responsible for the secretory function of NE-like PCa cells and whether the resulting cell-cell communication has an influence on the development of resistance to therapy.

Our results in this paper suggested that neuropilin-2 (NRP2), a transmembrane, non-kinase receptor belonging to the neuropilin (NRP) family (Dutta et al., 2016b; Roy et al., 2018; Stanton et al., 2013), is important for the cellular secretory functions. Previous studies, including several reports published by our group, have suggested that NRP2 promotes metastasis and is associated with poor cancer prognosis (Roy et al., 2018; Stanton et al., 2013; Borkowetz et al., 2020; Schulz et al., 2019). In this current study, we have identified significant NRP2 expression in NE-like PCa patient tissues. Our *in vitro* experiments and *in vivo* studies suggested that, by regulating secretory function, NRP2 promotes growth and

survival of NE-like PCa upon treatment with chemotherapeutic drugs. Our study identifies a novel NE-like PCa-specific mechanism of NRP2 in conferring therapy resistance to cancer cells and raises an opportunity to develop an NRP2 inhibitor for future therapeutic efficacy.

RESULTS

NRP2 is highly expressed in human NE-like PCa

NRP2 expression was analyzed in a tumor microarray (TMA) obtained from the Prostate Cancer Biorepository Network (PCBN) (Labrecque et al., 2019), which includes 70 visceral (including liver, lungs, lymph node, and kidney) and 51 bone metastatic cores from 45 castration-resistant rapid autopsy patients with clinical history. Thirty percent of the patients in this PCBN mCRPC cohort had undergone NE differentiation (NED) during the progression of PCa (Figure 1A). Interestingly, 87% of the patients with NE-like PCa having visceral and bone metastasis showed high expression of NRP2 with immunohistochemistry (IHC) scores 2 and 3 (Figures 1B and 1C). We further analyzed NRP2 expression in patient cohorts from the Stand Up to Cancer/Prostate Cancer Foundation (SU2C-PCF) (Abida et al., 2019), and a prospective clinical trial (identifier: NCT02432001) (Aggarwal et al., 2018). Each patient of these cohorts had originally been assigned with a NE PCa (NEPC) score (Abida et al., 2019; Aggarwal et al., 2018). NEPC score was calculated based on the presence of a small-cell population in the samples, expression of canonical NE markers, and AR status (Abida et al., 2019; Aggarwal et al., 2018). In these cohorts, we found that NRP2 expression was either maintained (Aggarwal et al., 2018) (Figure S1A), or elevated (Abida et al., 2019) (Figure 1D) in NE-like PCa patients. We further analyzed the single-cell RNA sequencing (RNA-seq) data of genetically engineered mouse model of advanced AR-negative PCa (Brady et al., 2021) to evaluate if NRP2 upregulation is also observed in PCa animal model. Interestingly, mice with poorly differentiated adenocarcinoma including NE transdifferentiation had significantly higher expression of NRP2 (Figure 1E). Overall, our analyses of patient and animal samples/databases demonstrated upregulation of NRP2 in poorly differentiated advanced PCa, including NE-like PCa.

Development and characterization of NE-like PCa cells

To test whether NRP2 can be a potential target against NE-like therapy-resistant PCa, we developed and characterized NE-like PCa cells in our laboratory. Previous studies highlighted that simultaneous loss of function of *RB1* and *TP53* genes often leads to the transdifferentiation of prostate adenocarcinoma into the NE-like phenotype (Ku et al., 2017; Mu et al., 2017). Upon NE-like transdifferentiation, prostate epithelial cells develop long neurite-like branched processes (Sang et al., 2016) with concomitant expression of markers, such as CHGA, Syp, AURKA, SOX2, N-Myc, ASCL1, and NSE (Beltran et al., 2016; Ku et al., 2017). During such transformation, AR-dependent PCa cells become independent of the AR axis for their survival, and eventually resist the second-generation AR-targeted therapies (Mu et al., 2017; Beltran et al., 2011, 2016; Ku et al., 2017). To get the molecular insights of the therapy resistance and identify potential molecular targets against NE-like PCa, we developed two cell line models. First, we used an mCRPC cell line, C4–2, which is an AR-responsive line, and knocked down RB1 and TP53 genes using shRNA to develop stable C4–2 RB1 and TP53 double-knockdown (DKD) cells. The idea

was to mimic the phenotype associated with NE-like transdifferentiation upon RB1 and TP53 simultaneous loss of function. Second, we utilized another advanced mCRPC cell line, C4–2B, and cultured it under exposure of 20 μM enzalutamide for 12 weeks to develop C4–2B enzalutamide-resistant (ER) cells. This mimics the NE-like lineage switch upon prior exposure to second-generation AR-targeted therapies. The two developed cell lines were characterized for NE-like features (Figure 2).

C4-2 RB1 and TP53 DKD cells develop NE-like phenotype—We observed that *TP53* and *RB1* genes were efficiently knocked down in C4–2 RB1 and TP53 DKD cells (Figures 2A and S1B). The cells developed long neurite-like branched processes (Figure S1C), suggesting attainment of NE-like morphology (Sang et al., 2016). We have further characterized those neurite structures by staining them with neurite-specific β3-tubulin (Figure 2B). We performed RNA-seq analyses of the adenocarcinoma cells (C4–2) and the developed NE-like PCa cells (DKD) to characterize the development of NE-like features. Our RNA-seq data revealed that REST-repressed genes, such as *SYP*, *CHGA*, and *INSM1*; transcription factors regulating NE differentiation, such as *SOX2*, *POU3F2*, and *NKX2–1*; and other genes involved in NE-like cancers, such as *NCAM1* and *MYCN* were significantly upregulated in the developed NE-like cells. On the other hand, AR, and other AR-regulated genes, such as *KLK3*, *CHRNA2*, and *NKX3–1*, were significantly downregulated in the NE-like PCa cells compared with adenocarcinoma (Figure 2C). These genetic signatures were previously reported to be present in NE-like PCa and in cancer cells undergoing NE-like transdifferentiation (Labrecque et al., 2019; Mu et al., 2017; Beltran et al., 2016). We validated our RNA-seq data using real-time PCR and western blot to check the expression of canonical NE markers (Figures 2D and S1D). Interestingly, we found either low or no expression of AR and its downstream target in the DKD cells compared with the control (Figures S1E and S1F), suggesting an AR-independent survival mechanism in these cells. We checked whether these cells developed resistance to enzalutamide following *RB1* and *TP53* depletion, as observed in the PCa patients (Labrecque et al., 2019; Ku et al., 2017; Beltran et al., 2016; Tritschler et al., 2017; Nadal et al., 2014). Indeed, the cells developed significant resistance to enzalutamide compared with control (Figure S1G). Together, the above observations suggested the development of NE-like characteristics in DKD cells. We then evaluated the NRP2 expression in the developed NE-like PCa cells. Interestingly, NRP2 was highly upregulated upon *RB1* and *TP53* depletion in the cells (Figure 2E), suggesting the presence of the active NRP2 axis in the NE-like DKD cells. We then evaluated if NRP2 is involved in NE-like transdifferentiation by overexpressing NRP2 in adenocarcinoma cells and observed any changes in NE-marker expression. Significant changes in NE markers were not observed upon NRP2 overexpression in adenocarcinoma cells (Figures S1H and S1I). Therefore, these results suggested that NRP2 is upregulated in PCa cells during NE-like transdifferentiation but it is not an inducer of the cellular process leading to lineage switch.

C4–2B ER cells attain NE-like characteristics—The developed C4–2B ER cells also attained NE-like cell morphology (long neurite-like branched processes) (Figure S1J). We characterized the cells by checking the expression of REST-repressed genes, such as *SYP* and *CHGA*; transcription factors regulating NE differentiation, such as *SOX2*; and

other genes implicated in NE-like differentiation, such as *AURKA*, *NSE*, and *MYCN* (Figures 2F and S1K). Our data revealed a downregulation of both *RB1* and *TP53* protein expression upon prolonged exposure to enzalutamide (Figure 2G). NRP2 protein expression was upregulated in C4–2B ER cells (Figure 2H), so we used these cell lines to test whether NRP2 can be a potential molecular target in NE-like therapy-resistant PCa.

In addition, we used *de novo* NEPC cell line, NCI-H660, for further validation of our results. NRP2 expression was also found to be significantly high in NCI-H660 cells (Figure S1L).

NRP2 depletion increases the efficacy of the front-line chemotherapeutic agents

Our study showed that DKD is significantly resistant to docetaxel compared with C4–2 control (Figure S2A). We further observed that NRP2 depletion significantly increased the efficacy of this cytotoxic drug as confirmed by the cell death assays (Figure 3). Initially, we checked the half maximal inhibitory concentration (IC_{50}) of docetaxel alone in DKD cells (Figure S2B) and chose a dose (10 nM) close to IC_{20} for our subsequent experiments, where 80% of cells were still viable. We used two different NRP2-specific small interfering RNAs (siRNAs) for our cell death experiments. Both the siRNAs showed significant NRP2 depletion in DKD cells and could enhance cell death at a similar level following docetaxel treatment, suggesting the on-target effect of NRP2 depletion (Figures 3A–3C). Further, overexpression of NRP2 in NRP2-knockdown DKD cells reverted its chemo-resistant phenotype, confirming the effect of NRP2 in promoting docetaxel resistance of NE-like PCa cells (Figures 3D–3F). Moreover, NRP2 depletion significantly increased the ability of docetaxel to hinder the colony formation of NE-like PCa cells (Figures 3G–3I). In addition, we performed the colony formation assays with DKD (NE-like cells) under the influence of VEGF-C, the ligand of NRP2. Our results demonstrated that the addition of recombinant VEGF-C significantly increased both the number and size of the colonies (Figures S2C and S2D). NRP2 ablation in the presence of exogenous VEGF-C could reduce the number and especially the size of the colonies (Figures S2C–S2E). Our results thus indicated that NRP2 ligands such as VEGF-C secreted by the surrounding cells in the microenvironment can promote the tumorigenic potential of cancer cells, and targeting NRP2 could decrease their tumorigenicity.

We also performed MTT assay and found that NRP2 depletion increased the efficacy of docetaxel (Figures S2F and S2G), recapitulating the results obtained from the above-mentioned cell death analyses. Similarly, NE-like C4–2B ER PCa cells were also highly resistant to docetaxel (Figures S2H and S2I), and NRP2 depletion significantly increased docetaxel efficacy in C4–2B ER cells (Figures S2J and S2K). These results demonstrate that, despite docetaxel therapy having been found to be less effective against the NE-like PCa (Akamatsu et al., 2018), its efficacy can be significantly improved if combined with NRP2 depletion.

We next tested whether targeting NRP2 can increase the efficacy of platinum chemotherapy-etoposide combination in NE-like PCa. Since NE-like PCa is resistant to docetaxel, platinum chemotherapy in combination with etoposide is an option to manage patients with NE-like phenotype (Akamatsu et al., 2018; Tritschler et al., 2017). Therefore, cisplatin and etoposide were tested for their efficacies in DKD cells, with and without NRP2 knockdown

(NRP2 KD). MTT assay revealed that the efficacy of cisplatin-etoposide combination was significantly increased when NRP2 was depleted in the cancer cells; i.e., lower dose of the platinum-etoposide doublet therapy is required to obtain potent cytotoxic effect (Figure S2L).

NRP2 depletion increases the efficacy of chemotherapy *in vivo*

NRP2 depletion increased the efficacy of platinum chemotherapy-etoposide doublet—A subcutaneous PCa mouse model was used to evaluate the efficacy of cisplatin-etoposide doublet therapy upon NRP2 depletion. For this, we have developed NE-like DKD cells that stably express shNRP2 (DKD-shNRP2) under the control of doxycycline (Dox) (Figure S3A). DKD-shNRP2 cells (1×10^6 cells) were implanted into the right flank of athymic nude mice. Once the tumors became palpable, animals were randomly divided into four groups (n = 5). The first group acts as a control. The second group received Dox (2 mg/mL) in water (2% sucrose) to deplete NRP2 in the cancer cells. In the third group, cisplatin (5 mg/kg body weight) and etoposide (8 mg/kg body weight) were administered (intraperitoneally [i.p.]) on day 1 and day 2, respectively, on a weekly basis for 3 weeks. The fourth group received both Dox in water and cisplatin-etoposide doublet. Tumors were regularly monitored, and tumor size was measured over the period until sacrifice. We observed that the growth of NE-like tumors in mice was slower initially. However, once formed, the tumors became very aggressive and grew persistently. A similar trait was reported previously for NE tumors, including NE-like PCa (Guo et al., 2019; Benten et al., 2018). Depletion of NRP2 along with the doublet therapy significantly reduced the tumor volume compared with control, only doublet therapy, and only NRP2 depletion, respectively (Figures 4A and S3B). In addition, tumor growth curve was constructed by plotting the tumor volumes of the four groups over the duration of treatment (Figure 4B). We observed that NRP2 depletion or the chemotherapeutic treatment alone can reduce the tumor growth; however, growth stall was profound in the NRP2-depleted group simultaneously receiving chemotherapy. NRP2 knockdown (Figures S3C and S3F), cancer cell proliferation, and cell death upon NRP2 depletion in combination with doublet therapy were evaluated by IHC. Ki67 staining was reduced in groups receiving chemotherapy and NRP2 knockdown alone; however, significant reduction of proliferation was observed in the group receiving simultaneous NRP2 knockdown and doublet therapy treatment compared with control (Figures S3D and S3G). On the other hand, NRP2 depletion significantly increased the efficacy of the cisplatin-etoposide doublet to induce cell death as demonstrated by the cleaved caspase-3 staining (Figures S3E and S3H).

NRP2 knockdown increased the efficacy of docetaxel—As bone is one of the major metastatic sites of advanced PCa, including NE-like PCa (Aggarwal et al., 2018; Conteduca et al., 2019), we decided to test the effect of NRP2 depletion in tumor growth in bone. Therefore, we injected DKD-shNRP2 cells into the bones of athymic nude male mice by intra-tibial injection. While C4–2 cells do not grow in the bone, interestingly, the DKD cells showed tumor formation in mouse bone, as confirmed by histological analyses (Figure 4). To test the role of NRP2 depletion on tumor growth, mice were randomly divided into four treatment groups with 10 mice in each group. The first group acts as a control. The second group received Dox (2 mg/mL) in water (2% sucrose) to deplete

NRP2 in the cancer cells. In the third group, docetaxel (5 mg/kg body weight, once every 7 days for 3 weeks) was injected by the i.p. route. The fourth group received both docetaxel injection and Dox in water. Dox-induced knockdown of NRP2, cancer cell proliferation, and cell death upon NRP2 depletion in combination with docetaxel were evaluated. NRP2 was efficiently knocked down upon Dox addition as revealed by IHC analysis and real-time PCR (Figures S3I–S3K). NRP2 depletion significantly increased the efficacy of docetaxel to inhibit NE-like PCa cell proliferation, and to exert profound cytotoxic action *in vivo*. NRP2 knockdown in combination with docetaxel significantly reduced the proliferation of NE-like PCa cells compared with control, only docetaxel treatment, and only NRP2 depletion, respectively (Figures 4C and 4F). In addition, the mouse bones having NRP2 knockdown in combination with docetaxel treatment were associated with more necrotic areas than the other three groups (Figures 4D and 4G). Moreover, cleaved caspase-3 staining revealed that NRP2 knockdown significantly increased the docetaxel-induced cell death compared with the control group as well as the groups under only docetaxel treatment and only NRP2 depletion (Figures 4E and 4H). Overall, our *in vivo* data demonstrated that the anti-tumorigenic actions of cisplatin-etoposide doublet as well as docetaxel are significantly increased upon NRP2 depletion in the NE-like therapy-resistant PCa, recapitulating our *in vitro* results.

NRP2 confers chemo-resistance to the surrounding cancer cells in paracrine manner

Transformed cancer cells in NE-like PCa share neural cells and secretory phenotype (Rindi and Wiedenmann, 2020). Thus, NE-like cells gain the ability to secrete biogenic amines, neuropeptides, peptide hormones, growth factors, and cytokines to establish cell-cell communication within the tumor microenvironment (TME) (Wiedenmann et al., 1998). Attainment of such a secretory phenotype to establish a crosstalk within the TME gives the NE-like cancer cells a survival advantage under stress (Laskaratos et al., 2021; Cives et al., 2019). Therefore, we tested whether the secretory pathways and molecular mediators to establish cellular communications are also enriched in NE-like PCa. Interestingly, functions related to secretion and players mediating cellular crosstalk were significantly enriched in patient cohorts with NE-like differentiation (SU2C-PCF) (Abida et al., 2019) as well as in NE-like DKD cells, as revealed by the pathway analyses of the respective RNA-seq data (Figures 5A and 5B). Previously, we have reported NRP2's function in vesicular trafficking and endosomal recycling processes (Roy et al., 2018; Dutta et al., 2016a), indicating its role in mediating secretory functions in the cancer cells. Hence, we evaluated whether NRP2 upregulation in the NE-like PCa cells has any role in the secretory phenotype of the cells, and thus in their enhanced survival. We performed co-culture experiments, where adenocarcinoma as well as NE-like PCa cells were co-cultured with another set of NRP2 +/− NE-like PCa cells, to understand if the NE-like PCa cells transmit NRP2-mediated pro-survival signals to the surrounding adenocarcinoma and NE-like cells. Both NE-like (Figures 5C and 5F) adenocarcinoma (Figures 5D and 5G) cells co-cultured with NE-like PCa cells having NRP2 showed higher cell viability compared with cells co-cultured with NE-like PCa cells having NRP2 knocked down, under the treatment with docetaxel. We also depleted NRP2 in an NEPC cell line, NCI-H660, collected the NRP2 +/− conditioned media (CM), and cultured adenocarcinoma cells under both the CM. While NRP2-positive CM could protect the adenocarcinoma cells from therapeutic pressure, cells cultured under

NRP2-depleted CM were sensitive to chemotherapy (Figures S4A and S4B). pAKT (Ser 473) levels were found to be significantly downregulated both in NE-like (Figures 5I and S4C) and adenocarcinoma (Figures 5J and S4D) cells co-cultured with NRP2-deficient NE-like PCa cells, suggesting the presence of NRP2-mediated pro-survival signal in the cancer cells present in the tumor milieu. Interestingly, the difference in the survival of adenocarcinoma cells upon docetaxel treatment was not observed when they were co-cultured with another set of adenocarcinoma cells under NRP2 +/− conditions (Figures 5E and 5H). We then overexpressed NRP2 in adenocarcinoma cells, collected the CM, and cultured another set of adenocarcinoma cells to check response to therapy. Interestingly, NRP2 overexpression in adenocarcinoma cells could not provide resistance to another set of adenocarcinoma cells against therapy (Figures S4E–S4G). Overall, the results suggested a function of NRP2 in NE-like PCa cells to regulate secretory phenotype and establish cell-cell communication in a paracrine manner to regulate survival of the surrounding cancer cells under chemotherapeutic stress.

NRP2 regulates exocytosis in the NE-like PCa cells by controlling the vesicular fusion pathway

As we observed NRP2 downregulation affect the paracrine communication among the cells, we evaluated whether inhibition of NRP2 has any effect on vesicular fusion signature and therefore on the regulation of secretory phenotype in the NE-like cells. For that, we conducted vesicle-associated membrane protein 2 (VAMP2) staining. Soluble N-ethylmaleimide-sensitive factor attachment proteins receptor (SNARE)-mediated exocytosis is important for the release of secretary molecules by NE cells (Somasundaram and Taraska, 2018). VAMP2 or synaptobrevin is a vesicle-associated SNARE, which, in association with other plasma membrane-associated SNAREs, promotes fusion of secretory vesicles to the plasma membrane. The vesicles then release their content into the extracellular milieu (Rindi and Wiedenmann, 2020). To understand the mechanism of how NRP2 confers chemo-resistance to the surrounding cancer cells in paracrine manner, we investigated the localization of VAMP2-positive exocytic vesicles in the NE-like PCa cells and compared with adenocarcinoma cells. While VAMP2-positive vesicles were found to be diffused and mainly located in the perinuclear region in C4–2 (Figure 6A), they were predominantly localized around the plasma membrane in both DKD and C4–2B ER cells (Figures 6B and S4H). The result suggests an active exocytosis process in NE-like PCa cells in comparison with adenocarcinoma. Interestingly, NRP2 depletion did not significantly change VAMP2 localization in C4–2 (Figure 6A). However, it significantly reduced VAMP2's membrane localization both in DKD and C4–2B ER cells (Figures 6B, 6C, and S4H). We also checked the VAMP2 protein levels in the NE-like PCa cells compared with adenocarcinoma cells. The expression level of VAMP2 was unchanged in NE-like PCa cells compared with adenocarcinoma (Figures S4I). Our result thus indicates the involvement of NRP2 in the translocation of VAMP2-positive vesicles to the cytoplasmic membrane and thus their fusion to the cell membrane in the NE-like PCa cells. We also performed a co-culture experiment like is the one described in the previous section, where NE-like cells were co-cultured with VAMP2 +/− NE-like PCa cells. We observed higher cell death when cells were co-cultured with VAMP2-deficient NE-like cells in combination with docetaxel treatment (Figures 6D and 6E). Similarly, a decrease in pAKT (Ser 473) level was

observed in cancer cells co-cultured with VAMP2-knockdown NE-like cells (Figures 6F and S4J). We also overexpressed NRP2 in adenocarcinoma cells to evaluate VAMP2-positive vesicle localization. Interestingly, NRP2 overexpression could not significantly change the localization of exocytic vesicles from the perinuclear region to the plasma membrane in adenocarcinoma cells (Figures S4K and S4L). Together, our observations indicate NRP2's ability to regulate the vesicular fusion pathway in NE-like PCa cells and that its inhibition decreases exocytosis in NE-like PCa cells.

We then questioned how NRP2 gains the ability to regulate exocytosis mainly in NE-like PCa cells. To understand the underlying molecular mechanism by which NRP2 regulates such secretory functions, we investigated the patient database to determine which molecular events are preferentially altered in NE-like cancer. We analyzed a treatment-refractory mCRPC patient cohort having PCa patients with NE-like phenotype (GSE126078) (Labrecque et al., 2019). Through gene set enrichment analysis (GSEA), we identified an array of genes that are upregulated in NE-like PCa compared with adenocarcinoma (Figure 6G). They regulate pathways involved in vesicular secretion, exocytosis, and neurotransmitter release (Figure S5). Similar gene profiles were also identified to be upregulated in NE-like PCa when we analyzed the SU2C-PCF patient cohort (Abida et al., 2019) (Figure 6H). Interestingly, the majority of the genes found in the analysis of patient cohorts were also upregulated in DKD cells compared with C4–2 when we re-evaluated our RNA-seq data described previously in Figures 2A, 5B, and 6I. We speculated whether the expression of these genes is regulated by NRP2. Our RT-PCR result (Figure 6J) indicated that synapsin-1 (*Syn1*) among the identified candidate genes was downregulated following NRP2 knockdown. This result was further confirmed in protein level by western blot in DKD cells following the depletion of NRP2 (Figure 6K). The above observations thus suggested the upregulation of molecular mediators such as Syn1 in NE-like PCa, which enhances its secretory phenotype. Syn1 tethers the reserve pool of secretory vesicles to the cytoskeleton and thus plays an important role in promoting their migration to the active zone of the cell membrane where secretion occurs (Orlando et al., 2014; Bloom et al., 2003; Chenouard et al., 2020). Thus, NRP2, by regulating Syn1 expression in NE-like PCa cells, controls the vesicular fusion and exocytosis that is important to establish paracrine communication among the cancer cells in the tumor milieu and to confer therapy resistance.

Characterization of NRP2-regulated secretome in NE-like PCa cells

We performed mass spectrometric analysis of the spent media of NE-like PCa cells with and without NRP2 depletion to identify the biomolecules (secretome) whose secretions are dependent on NRP2. The secretome we obtained in NE-like DKD cells under control conditions matches 63% with the published secretome for NE tumor (Wang et al., 2019), showing similarityof the secretory proteins across the NE-like cancer cells. Interestingly, the analysis of RNA-seq results of NE-like cells (DKD) and its syngeneic adenocarcinoma cells (C4–2) showed that the expression of many of these secretory products is significantly enhanced in NE-like cells (Figure S6A), suggesting specific functions of these proteins in NE-like PCa. Pathway analysis of these secretory proteins in the control-spent media suggested that they regulate functions such as cellular metabolic process, amide biosynthesis, protein translation, vesicle-mediated transport, exocytosis, mitotic cell cycle

process, axon guidance, and extracellular exosomes (Figure 7A). Enrichment of these pathways in the secretome is typical for NE tumor cells and is important to maintain their secretory and functional characteristics (Wang et al., 2019). Many of the proteins in the secretome, such as TGFB1, IGF2BP2, CNTN1, NCAM1, EPHA7, NRAS, and ABCE1, which have roles in cancer progression, aggressiveness, and therapy resistance (Li et al., 2020; Shiota et al., 2021; Xu et al., 2019; Liang et al., 2020; Guan et al., 2020; Huang et al., 2010; Kara et al., 2015; Wang et al., 2019), were downregulated in the secretome upon NRP2 knockdown (Figure 7B). To confirm that NRP2 depletion affected the secretion but not the synthesis of these secretory products, we analyzed our RNA-seq result of DKD cells following the knocking down of NRP2. Gene expressions of most of the secretory products were not significantly affected following NRP2 depletion, confirming our finding that NRP2 regulates the secretion of these proteins in NE-like PCa cells (Figure 7C). We also observed the upregulation of several cytokines in NE-like cancer cells compared with adenocarcinoma cells in our RNA-seq data, which have roles in tumor progression (Figure S6B). However, those cytokines were not detected in our mass spectrometric analysis. Therefore, we performed a separate cytokine array to understand whether NRP2 also regulates their secretion. Our results suggested that some cytokines, such as IL-8, PTX3, PLAUR, and VEGF, were significantly less in the spent media of NRP2-knockdown NE-like PCa cells compared with control (Figure 7D). Our RNA-seq data once again confirmed that the expression of majority of these cytokines was not significantly changed upon NRP2 depletion (Figure S6C). These cytokines are known to regulate cancer cell growth, proliferation, invasion, migration, and metastasis to impart aggressiveness to the tumor cells (Bakouny and Choueiri, 2020; Gilder et al., 2018). Notably, IL-8 was shown to be highly upregulated in NE tumor cells to promote androgen-independent growth of PCa (Huang et al., 2005). IL-8 was also present in the previously published secretome of NE tumor (Wang et al., 2019). Considering the importance of IL-8 in androgen-independent advanced PCa, we performed experiments to address whether IL-8 can be one of the NRP2-regulated secretory molecules that protect PCa cells from chemotherapy. We observed the expression of the IL-8 receptors, especially CXCR2, in the RNA-seq analysis of adenocarcinoma and NE-like PCa cells, and their ligand-induced activation in both of them (Figure S6D). In addition, we also cultured the adenocarcinoma cells under NRP2 +/− CM of NE-like PCa cells to evaluate IL-8 receptor activation (phosphorylation of CXCR2 as readout) in adenocarcinoma cells. As expected, the CM of NRP2-depleted NE-like PCa cells was less capable of activating IL-8 receptors than the control (Figure S6E). Moreover, exogenous addition of IL-8 in NRP2-depleted NE-like cells could partially protect the PCa cells from chemotherapy-induced cell death (Figures S6F and S6G). Together, these results thus suggested that IL-8 is one of the key NRP2-regulated secretory factors of NE-like PCa cells, which enables the NE-like cells to promote resistance to chemotherapy in the neighboring cancer cells. To further evaluate NRP2's role in the regulation of secretory phenotype in PCa cells, we collected the CM of the NRP2-expressing adenocarcinoma cells (C4–2B), performed mass spectrometric analysis, and compared with that performed for NE-like PCa cells. Our results indicate a decrease of secretory factors in adenocarcinoma CM compared with that of NE-like PCa cells (Figure S7A). Since some of the cytokines, including IL-8, was not detected in our mass spectrometry studies, we tested the presence of cytokines in the CM of NRP2-expressing and NRP2-knockdown adenocarcinoma (C4–2B) cells by cytokine

array analysis. Surprisingly, we observed that the level of some of the cytokines, including IL-8, were partially decreased in the CM of NRP2-knockdown adenocarcinoma cells, while cytokines such as VEGF were unchanged in either of these conditions (Figure S7B). Our results thus suggest that NRP2 in addition to NE-like cells can control the secretion of some of the cytokines in aggressive adenocarcinoma such as C4–2B. To answer how NRP2 can control the secretory function in C4–2B, which is also an adenocarcinoma, although more aggressive than C4–2, we evaluated the localization pattern of VAMP2-positive secretory vesicles in C4–2B. Our results indicated that VAMP2-positive vesicles can be seen at some specific protruding regions of the cell membrane of C4–2B (Figure S7C). Such a distribution pattern of VAMP2-positive vesicles was not seen in C4–2 (Figure 6). Interestingly, NRP2 depletion in C4–2B affected the localization of VAMP2-positive vesicles (Figure S7C). Our results thus showed that adenocarcinoma at its advanced stages can also gain some degree of secretory ability. The question then can be raised why we could not detect any difference in chemotherapy-induced death of C4–2 when they were co-cultured with NRP2-expressing and NRP2-depleted C4–2B (Figure 5). One explanation could be that C4–2B secretes a lower level of several growth factors/cytokines as it expresses those factors at significantly low level compared with DKD (Figure S7A). Interestingly, our data indicated that IL-8 expression is comparable between C4–2B and DKD (Figure S7D). We therefore compared IL-8 level in the CM of NE-like PCa cells with both C4–2B and C4–2 and observed that IL-8 is present at significantly higher level in the CM of DKD and NCI-H660 compared with C4–2B and C4–2 (Figure S7E). Our results thus suggested that advanced adenocarcinoma can gain some secretory ability, but it is not comparable with the robust NRP2-regulated secretory function of NE-like cells.

Overall, our results demonstrated that NRP2 is highly upregulated in NE-like PCa, which is required for secretory function of the NE-like cells to protect themselves from chemotherapy through autocrine and paracrine mechanism. Our results further indicated that NRP2 is not the sole regulator of the secretory function; rather, it works along with other molecular modulators. NRP2 overexpression in adenocarcinoma cells therefore is not sufficient to induce any secretory function. The likely reason is the absence of other necessary molecular mediators for secretion. The proposed mechanism is illustrated in Figure 7E.

DISCUSSION

The transdifferentiation of prostate adenocarcinoma to attain NE-like characteristics has recently received more attention as an important mechanism for the development of an aggressive therapy-resistant PCa phenotype (Ku et al., 2017; Beltran et al., 2016; Tritschler et al., 2017; Abida et al., 2019; Labrecque et al., 2019; Patel et al., 2019). Recent investigation on an SU2C-PCF patient cohort (Abida et al., 2019) has revealed the presence of some altered genes commonly upregulated in patients with NE-like phenotype. Interestingly, these genes regulate some important neuronal functions (Abida et al., 2019), as well being implicated in the poor prognosis in cancer progression, and thus they become lucrative candidates for further study. One such molecule is NRP2 (Roy et al., 2018; Stanton et al., 2013; Borkowetz et al., 2020; Schulz et al., 2019).

Currently, platinum-based chemotherapies are used to treat small-cell NE tumors and have shown sensitivity in the range of 10%–50% (Aparicio et al., 2013; Flechon et al., 2011). For non-small-cell variants of NEPC, both taxane-based and platinum chemotherapies are used (Aparicio et al., 2013). Regardless of some initial chemosensitivity, the overall outcome to those therapies for treating NE-like PCa is poor, which thus warrants novel treatment options. In this context, we tested whether targeting the NRP2 axis, especially in combination with chemotherapies, can enhance the treatment response against NE-like PCa. Our *in vitro* and *in vivo* studies suggested that depletion of NRP2 significantly sensitized NE-like PCa cells toward the combined treatment of cisplatin and etoposide. Our results thus highlighted the potential benefit of targeting NRP2 axis to sustain the chemosensitivity of platinum-based chemotherapeutic regimens, which, therefore, is expected to yield a better overall outcome for NE-like PCa patients with small-cell morphology.

Moreover, NRP2 depletion significantly increases the efficacy of docetaxel in the NE-like PCa cells, the first-line chemotherapy they typically are resistant to (Tritschler et al., 2017; Akamatsu et al., 2018). Once again, we tested both *in vitro* and *in vivo* models to test the efficacy of docetaxel in NE-like PCa upon NRP2 axis inhibition. Bone is one of the major metastatic sites for mCRPC, including t-NEPC (Labrecque et al., 2019; Liu et al., 2020). Although previous reports indicated that t-NEPC has a preference to metastasize in visceral sites, the recent SPARTAN trial concluded that there were no significant differences between the frequency of visceral and bone metastases of t-NEPC patients (Smith et al., 2018). Our results suggest that NRP2 is expressed at high level in tumors metastasized to bone in mCRPC, including NE-like PCa patients. Therefore, in our *in vivo* study, we used an intra-tibial model to show that docetaxel treatment following NRP2 significantly reduced NE-like PCa cell proliferation and induced cell death of NE-like PCa cells. Our findings thus create an opportunity of developing a better patient management strategy by targeting NRP2 in combination with docetaxel.

Like *de novo* NE cells, it is believed that PCa cells with NE differentiation also regulate their own functions and the functions of the surrounding cells (such as adenocarcinoma) through autocrine, paracrine, endocrine, and neurocrine mechanisms. The secretory ability of NE-like cells is therefore critical for these functions (Butler and Huang, 2021). We observed that NRP2 has role in regulating the secretory function of NE-like PCa cells, which thus regulates paracrine communication among the cancer cells in the tumor microenvironment. Our mass spectrometric analysis identified several proteins enriched in the secretome of NE-like PCa cells, such as growth factors (such as TGFB1 and IGF2BP2), cytokines (such as IL-8, PTX3, PLAUR, and VEGF), and ATP-binding cassette protein (ABCE1), which were decreased when NRP2 was knocked down. TGFB1 functions as a tumor promoter in metastatic PCa and leads to poor prognosis in patients with androgen deprivation therapy (Shiota et al., 2021). Earlier, IL-8 was reported to be associated with aggressive nature of NE-like PCa (Huang et al., 2005). A mitogenic and angiogenic cytokine, IL-8, is detected in high amounts in the serum of advanced PCa patients and promotes NE differentiation of prostate tumors (Inoue et al., 2000; Koch et al., 1992). In this context, our data further validated that IL-8 is an important factor secreted by NE-like tumor that provides therapy resistance in the tumor microenvironment. Moreover, our results showed that NRP2 is one of the important molecular regulators of IL-8 secretion and thereby influences the development

of treatment-resistant PCa. As there are still limited opportunities for treatment of NE-like cancers in clinical setups, our result in this connection brings a new strategy by targeting NRP2 to sensitize such highly aggressive NE-like cancers to chemotherapies. Although we focused our study on IL-8, we are not ruling out the importance of other factors in association with the progression and development of therapy resistance in NE-like cancer. Reports have suggested that TGFB1 can lead to docetaxel resistance by transcriptionally upregulating an apoptosis suppressor, Bcl-2, and promotes PCa cells' switch from androgen dependence to androgen independence (Li et al., 2020; Lin et al., 2007). On the other hand, IGF2BP2 promotes tumor growth and progression by activating the phosphoinositide 3-kinase/protein kinase B (PI3K/Akt) signaling pathway (Xu et al., 2019). Finally, ABCE1 stimulates tumor cell proliferation, inhibits apoptosis, and imparts therapy resistance in different cancers, including small-cell lung carcinoma, quite similar to NE-like PCa (Huang et al., 2010; Kara et al., 2015). Likewise, the other cytokines differentially expressed under NRP2 +/− conditions are also implicated in tumor progression and cancer cell survival (Rathore et al., 2019; Gilder et al., 2018; Zhan et al., 2013). Thus, NRP2 in NE-like PCa promotes the survival of both NE-like and adenocarcinoma cells, which often coexist in the advanced PCa tissues resistant to ARIs or first-line chemotherapies.

As a mechanism, our results suggested that NRP2 regulates the secretory phenotype in the NE-like PCa cells through Syn1. Syn1 ensures the availability of vesicles at the active zone of the synapse by tethering vesicles to actin filament and other cytoskeletons (Orlando et al., 2014). NRP2 depletion leads to the downregulation of syn1, which results in impaired localization of the exocytic vesicles around the plasma membrane. Thus, NRP2 controls the secretory phenotype in the NE-like PCa cells and impedes paracrine communication mediated by the NE-like PCa cells by regulating Syn1. Therefore, this study identifies a novel mechanism of NRP2 in NE-like PCa cells, which aid in conferring therapy resistance to cancer cells and raises an opportunity to develop an NRP2 inhibitor for enhanced therapeutic efficacy against aggressive and therapy-resistant NE-like PCa. Of note, our results also suggested that NRP2 can control a similar secretory phenotype in NRP2-expressing advanced adenocarcinoma cells. However, the robust NRP2-regulated protective effect conferred by the paracrine signaling of the NE-like PCa cells is a combined effect of high NRP2 expression and accompanying molecular mediators of secretory pathways developed in the PCa cells upon NE transdifferentiation. We concluded that NRP2 is one of the important regulators in controlling the secretion of NE-like and aggressive adenocarcinoma, although these cells acquire the secretory ability upon lineage switch through a molecular mechanism independent of NRP2.

Overall, our results demonstrate that NRP2 regulates the secretory function of the NE-like PCa cells, which helps them to communicate with the surrounding heterogeneous cancer cells typically present in the NE-like PCa setting. Thus, NRP2 enhances the ability of the cancer cells present in the tumor milieu to resist therapeutic stress, whereas depletion of NRP2 enhances the efficacy of chemotherapies of NE-like PCa.

Limitations of the study

Treatment-refractory NE-like PCa represents a spectrum of disorder that carries various genetic and epigenetic modifications. Currently, there is no model including GEM or PDX that can represent these wide spectra of NE-like PCa. Using different *in vitro* and *in vivo* model systems, here we tried to mimic the diverse nature of NE-like cancer to address the common endocrine functions maintained by these cells. Since most of these NE-like cancers lack functional RB1 alone or in association with TP53 in their genomes, we have focused on NE-like tumors that possess this specific genotype. However, we agree that there are other NE-like PCa with specific genotypes, which were not represented by the model system.

STAR★METHODS

RESOURCE AVAILABILITY

Lead contact—Requests for further information and/or resources should be directed to and will be fulfilled by the lead contact, Samikshan Dutta (samikshan.dutta@unmc.edu).

Materials availability—All materials generated in this study are available from the any of the lead authors.

Data and code availability—RNA-seq data deposited at GSE202299. Mass spectrometry data are submitted in Mendeley Data (Mass Spectrometry_Sup_Prostate Cancer; Dutta, samikshan (2022), “Mass Spectrometry_Sup_Prostate Cancer”, Mendeley Data, V2, https://doi.org/10.17632/sx2fhffmt7.2). Any additional information required to reanalyze the data reported in this work paper is available from the Lead contacts upon request.

This paper does not report original code.

REAGENTS

Cell culture media- RPMI 1640 (Thermo Fisher Scientific, Gibco, NY, 11875093), DPBS, 0.25% (w/v) Trypsin, (100X), and Penicillin-Streptomycin (5,000 U/mLml) were acquired from ThermoFisher Scientific. Fetal bovine serum and goat serum were procured from GIBCO. For Wwestern blot, primary antibodies against NRP2 (R&D Systems, AF2215), AR (Cell Signaling, 5153), TP53 (Cell Signalling, 2524), RB1 (Cell Signalling, 9309), SYP (Cell Signalling, 36406), SOX2 (Cell Signalling, 23064), Synapsin-1 (Cell Signaling, 5297), IL-8 (R&D Systems, MAB208), NKX3.1 (Cell Signaling, 83700), GAPDH (Cell Signaling, 5174), Histone H3 (Cell Signaling, 5192), Rho-GDI (Cell Signaling, 2564) and HSC70 (B-6, sc-7298) were used. Donkey anti-goat IgG-HRP (Promega, V805A), goat anti-rabbit IgG-HRP (Invitrogen, 65–6120) and goat anti-mouse IgG-HRP (Invitrogen, 62–6520) were used as secondary antibodies. For immunohistochemistry, primary antibodies against NRP2 (Atlas Antibodies, HPA039980) and Ki67 (Cell Signaling, 9027) were used. Biotin conjugated goat anti-rabbit IgG (Invitrogen, 31820) was used as secondary antibody followed by Reagent A: Avidin (Thermo Scientific, 1852280) and Reagent B: Biotinylated HRP (Thermo Scientific, 1852310). ImmPACT DAB (Vector Laboratories, SK-4105) was used for protein visualization. For immunofluorescence and immunocytochemistry, primary antibody against Cleaved Caspase-3 (Cell Signaling, 9579), p-AKT (S473) (Cell

Signaling, 3787), VAMP2 (Cell Signaling, 13508), P-CXCR2 (Thermo Fisher Scientific, PA5–104850), B3-tubulin (Cell Signaling, 5568), and secondary Alexa Fluor 647 donkey anti-rabbit (Thermo Fisher A31573), and Alexa Fluor 488 goat anti-rabbit (Thermo Fisher A11008) antibodies were used. siRNA against human NRP2 and non-targeting control (ON-TARGET plus, smart pool) was bought from Dharmacon (Dharmacon RNA Technologies, L-017721–00–0010, LU-017721–00–005). siRNA against human VAMP2 was bought from Dharmacon (Dharmacon RNA Technologies, L-012498–00–0005). Recombinant human IL-8 was procured from R&D Systems (Cat# 208-IL). Reagents such as HEPES, KCl, DTT, NP-40, Glycerol, MgCl2, EDTA, PMSF, cyclosporine A, protease inhibitors such as aprotinin, and leupeptin were purchased from Sigma-Aldrich. Halt phosphatase inhibitor (1862495), Trizol and Powerup SYBR Green master mix were bought from ThermoFisher Scientific. cDNA kit was obtained from Roche, and primers from IDT. Proteome profiler array (Human XL cytokine Array kit; ARY022B) was procured from R&D Systems.

EXPERIMENTAL MODELS AND SUBJECT DETAILS

Retrospective study of human mCRPC and NE-like PCa—Commercially available mCRPC tumor microarray was procured from the Prostate Cancer Biorepository Network (PCBN; TMA number 92 A, B, C and D). The tissue microarray contained tumor cores obtained from different visceral and bone metastatic sites of forty-five mCRPC patients with known clinical diagnosis. Out of forty-five patients, fifteen (one-third) were clinically diagnosed with NE-like PCa. Expression of NRP2 in the TMA was evaluated by immunohistochemistry (described below), and the staining was validated by pathologist, Dr. Michael Muders, who also scored the TMA for NRP2. For gene expression data analysis, GSE32269, Stand Up to Cancer/Prostate Cancer Foundation) International Prostate Cancer Dream Team consortium, prospective clinical trial (identifier: NCT02432001) patient cohorts containg primary, mCRPC and NE-like PCa patient data were utilized.

Patient cohorts and animal model for bioinformatics data analysis—Publicly available RNA-seq data of the following human patient cohorts were analyzed: SU2C-PCF (Stand Up to Cancer/Prostate Cancer Foundation) International Prostate Cancer Dream Team consortium (Abida et al., 2019), a prospective clinical trial (Aggarwal et al., 2018) (identifier: NCT02432001), treatment refractory mCRPC patient cohort having PCa patients with NE-like phenotype (GSE126078) (Labrecque et al., 2019), and advanced AR negative prostate cancer mouse model (GSE151426).

Generation of C4–2 TP53, RB1 and TP53 + RB1 (DKD) knockdown cells—A panel of GIPZ TP53 and RB1 shRNA containing plasmids tagged with GFP (TP53-V3LHS_333919, 333920, 404717; RB1-V2LHS_130606, 340824, 340827) were purchased from Thermofisher scientific. Development of C4–2 cells containing TP53/RB1 and TP53 with RB1 shRNA was conducted as per manufacturer's protocol. Briefly, the lentivirus from each clone was generated by using HEK293T cells transfected with the shRNA containing plasmids. The generated lentivirus was transduced into C4–2 (kind gift from Prof. Allen Gao) followed by puromycin (Sigma-Aldrich) selection of the cells positive for each clone. The GFP-cells were then sorted by FACS. Following this, the clones were expanded and evaluated for the efficiency of knockdown of TP53 and RB1 at RNA level. Based on the

efficacy of knockdown of TP53 and RB1, the clones with highest knockdown were selected for all experiments.

Generation of C4–2B ER cells—C4–2B cells (kind gift from Prof. Allen Gao) were cultured under prolonged exposure of 20 μM enzalutamide for 12 weeks (31 passages) to develop C4–2B enzalutamide resistant cells.

METHOD DETAILS

Cell culture and transfection—The developed NE-like cells were cultured in RPMI 1640 with 10% FBS in the presence of antibiotics penicillin-streptomycin. Upon confluency, these cells were washed with DPBS and brief rinse with 0.25% (w/v) Trypsin-EDTA to detach the cells from the plate. The cells were collected in equal volumes of complete medium to neutralize the effect of trypsin. The cells were pelleted by centrifugation at 1000 g for 5 min. The cells are then suspended in fresh complete media and plated in a T-75 flask and cultured in a tissue culture incubator maintained at 37°C and 5% CO2. Cells were transfected using TransIT-X2 Transfection Reagent (Madison, WI, Mirus, MIR6000) (Dharmacon RNA Technologies, T-2005–02).

Western blot—Cells were lysed with ice-cold RIPA buffer (Boston Bioproduct, BP-115; pH 7.4) and combination of protease inhibitors, 20 μg/mL Leupeptin, 10 μg/mL Aprotinin, 1mM PMSF and Halt protease.

For separation of nuclear and post-nuclear fraction in osteoclasts, 250 μL of buffer A (10 mM HEPES pH 7.8, 10 mM KCl, 2 mM MgCl2, 0.1 mM EDTA, 10 μg/mL Leupeptin, 10μg/mL Aprotinin, 3 mM DTT, 1mM PMSF and Halt phosphatase inhibitor was added to each sample. Cells were scrapped, lysed properly with 26G and centrifuged at 13,500 RPM for five mins. The supernatant was separated from the pellet and used for protein analysis. Total protein was estimated using Bradford reagent and the samples were prepared by the addition of SDS sample buffer containing β-mercaptoethanol and boiled at 95°C for five minutes. The prepared samples were run on a precast 4–20% Mini-PROTEAN® TGX™ Gel (BioRad) and transferred on to a PVDF membrane (Life Technologies). The membrane was blocked in 5% non-fat dry milk in 1X TBST (1X Tris-Buffered Saline, 0.1% Tween 20) for at least 30 min and primary antibody diluted in 1X PBS was added and incubated overnight at 4°C with continuous shaking at low speed. On the next day, membrane was washed with 1X TBST for four times for 5min and incubated in appropriate dilution of secondary antibody conjugated with HRP for 1hr in 1X TBST, or in 5% non-fat dry milk in 1X TBST for anti-goat secondary antibody, with continuous shaking at low speed at room temperature. Following this, the membranes were washed in 1X TBST every 10 min for at least 10–12 times, and the protein bands were detected using a combination dilution of SuperSignal™ West Femto Maximum Sensitivity Substrate and SuperSignal™ Pico Maximum Sensitivity Substrate captured on an X-ray film.

Real-time quantitative PCR—Total RNA was isolated by adding 1mL of TRIzol Reagent (ThermoFisher Scientific, CA) per 1 million cells as per manufacturer's protocol and allowed to stand for 5 min at room temperature. Phase separation by chloroform

followed by RNA precipitation with ethanol was done. The supernatant obtained by centrifugation was decanted, and the pellet was air-dried briefly resuspended in UltraPure DNAse and RNAse free water (Life Technologies, 10977–015). The concentration and quality of the RNA were analyzed using Nanodrop Spectrophotometer. cDNA was synthesized with Transcriptor First strand cDNA synthesis kit (Roche Diagnostics Corporation) as per the instructions provided by the manufacturers. 1 μg RNA was used to generate cDNA. For real-time PCR, cDNA (50ng) was used, and each reaction was performed in duplicates in 25 μL volume in a 96-well PCR plates using SYBR green detection system (Applied Biosystems Group) in an ABI 7500 Fast and Real-Time PCR (2 min at 50°C, 10 min at 95°C and 40 cycles of 15 s at 94°C and 1 min at 60°C) with 200–300 nM concentration of primers. The list of the primers used in this study is listed in table the following table.

Gene	Forward	Reverse
36B4	ATGCAGCAGATCCGCATGT	TCATGGTGTTCTTGCCCATCA
NRP2	GTGAAGAGCGAAGAGACAACCA	GCAGTTCTCCCCACACTCTG
RB1	CTCTCACCTCCCATGTTGCT	GGTGTTCGAGGTGAACCATT
TP53-common 1	CCTCACCATCATCACACTGG	CACAAACACGCACCTCAAAG
CHGA	TGTCCTGGCTCTTCTGCTCT	CAACGATGCATTTCATCACC
Syp	GATGTGAAGATGGCCACAGA	TCAGCTCCTTGCATGTGTTC
SOX2	CAAGATGCACAACTCGGAGA	GCTTAGCCTCGTCGATGAAC
Ezh2	TGGGAAAGTACACGGGGATA	GCATTCACCAACTCCACAAA
Enolase 2 (NSE2)	TGGATCGGCAACTAAACCAT	TTCTGGACGTTCTTCTTTCACA
AURKA	CCTGAGGAGGAACTGGCATC	CAGAGAGTGGTCCTCCTGGA
MYCN	CAAAGGCTAAGAGCTTGAGC	GAACTCGACAGGGGACCGAT
ASCL1	AGAAGATGAGTAAGGTGGAG	AGTTCAAGTCGTTGGAGTAG
Synapsin1	TACCCCGTGGTTGTGAAGAT	GTCCTGGAAGTCATGCTGGT
Synapsin2	AACATCAGGTGGAGGACAG	AGGAGACAGGGCAGGAGT
SEPTIN1	TCTGTCAAGAAGGGGTTTG	CATAGAGGTTGGTGAGGAAG
SEPTIN6	CAGTATCCTTGGGGCACTGT	GTTGACCCGAATCAGCATCT
SCAMP5	AAATTTTACCGGGGAAGTGG	TGCTGCACATGTGGATTCTT
ARPC5	AGAGCCCGTCTGACAATAGC	CAATGGACCCTACTCCTCCA
CDC42	ACGACCGCTGAGTTATCCAC	GGCACCCACTTTTCTTTCAC
Rab3C	GAGCGCCTTGTGGATATCAT	TTCTGCTTTGCAGCAGTGAT

The expression was calculated relative to that of control cells and normalized with 36B4 measured under the same conditions (Applied Biosystems/Roche, Branchburg, NJ), using the 2–ΔΔCT method.

Colony formation assay—Cells were mixed in 0.3% Noble agar (in RPMI medium supplemented with 10% FBS) at 37°C and immediately plated at 5000 cells/well on the top of a solidified agar layer of the 6-well plates (0.5% Noble agar in the same growth medium). Media was supplemented every third day along with the respective treatments. After 21 days, colonies were stained with crystal violet solution (0.05% crystal violet-2% ethanol in

PBS) for 1 h followed by washing with PBS and then was photographed. The size of the colonies was measured using ImageJ.

Cell viability assay—Vybrant Apoptosis Assay Kit 7 was purchased from Molecular Probes (Invitrogen) and was used according to the manufacturer's protocol. Briefly, the cells were seeded at a density of 75,000 cells per well of a two-well chamber slide (LabTek Rochester, NY). NRP2 were depleted using siRNA and 24 h later the cells were treated with docetaxel (Mylan, NDC 67457–531–02). After 24 h of docetaxel treatment, adherent cells were washed with 1 × PBS and incubated with 1 μL of Hoechst 33342 and propidium iodide (PI) at room temperature for 15 min. The cells were viewed under a confocal microscope.

MTT assay—MTT assay was performed according to manufacturer's protocol (Cayman Chemical, 10009365). In brief, cells were seeded in a 96-well plate at a density of 5000 cells/well in 100 μL of culture medium. Cells were cultured in a CO_2 incubator at 37°C for 48 h 10 μL of MTT reagent was added to each well using a repeating pipettor, and mixed gently for one minute on an orbital shaker. The cells were then incubated for three to four hours at 37°C in a CO_2 incubator. After incubation, the formazan crystals were produced in the cells, which appeared as dark crystals in the bottom of the wells. 100 μL of crystal dissolving solution was added to each well, and was incubated for 4 h in a 37°C CO_2 incubator. A purple solution was produced. Absorbance was measured at 570 nm using a microplate reader.

***In-vivo* prostate cancer subcutaneous mouse model—**All animal studies were conducted in accordance with the University of Nebraska medical center IACUC guidelines. To evaluate the effect of NRP2 depletion on the efficacy of chemotherapy, we have developed stable shNRP2 expressing clones of C4–2 TP53 + RB1 double knockdown cells (DKD-shNRP2), where shRNA can be inducibly expressed upon administration of doxycycline (Dox). DKD-shNRP2 cells (1×10^6 cells) were implanted into the right flank of athymic nude mice. Once the tumors became palpable, animals were randomly divided into four groups (n = 5). Briefly, the first group acts as a control. The second group received doxycycline in water (2 mg/mL) to deplete NRP2 in the cancer cells. In the third group, cisplatin (5 mg/kg body weight) and etoposide (8 mg/kg body weight) were administered (i.p) on day 1 and day 2, respectively, on a weekly basis for three weeks. And, the fourth group received both doxycycline in water and cisplatin-etoposide doublet. Tumors were regularly monitored and tumor size was measured over the period of time until sacrifice. Tumor volume was calculated by using the formula: ½ ab^2 (Kersemans et al., 2013).

***In-vivo* prostate cancer bone metastatic mouse model—**All animal studies were conducted in accordance with the University of Nebraska medical center IACUC guidelines. To evaluate the effect of NRP2 depletion on the efficacy of chemotherapy, we have developed stable shNRP2 expressing clones of C4–2 TP53 + RB1 double knockdown cells (DKD-shNRP2), where shRNA can be inducibly expressed upon administration of doxycycline (Dox). The requirement of NRP2 for PCa growth in bone was tested by implanting DKD-shNRP2 cells in the tibia of immunocompromised mice and then knocking down NRP2 by Dox from cancer cells with or without concomitant docetaxel

administration. Briefly, DKD-shNRP2 cells stably expressing GFP-luciferase tagged shNRP2 under the control of doxycycline were injected intratibially in athymic nude male mice in the age group of 8–12 weeks purchased from Jackson labs. 100,000 cells per 30 μL PBS were injected into the left tibia of mice. The right tibia received PBS only. Tumor burden in the bone was monitored by IVIS imaging and after 4 days of injection, the mice were randomized into four groups with 10 mice in each group. The first group acts as a control and received sucrose in water. The second group received doxycycline in water (2 mg/mL) to deplete NRP2 in the cancer cells. The third group was injected intraperitoneally with docetaxel (5 mg/kg body weight: once every 7 days for three weeks) and sucrose in water. The fourth group received docetaxel injection and doxycycline in water. After 3 weeks, all mice were sacrificed and the tumor cells containing bones were obtained. Bone marrow from three bones from each group were used to sort tumor cells expressing GFP by flow cytometry. These tumors cells were processed to obtain RNA and Real-time PCR was conducted to check the efficiency of NRP2 depletion. The rest of tumor bearing bones were used for evaluating NRP2 knockdown efficiency by IHC. The tumor bearing bones were formalin-fixed for further processing and evaluation of cancer cell proliferation, apoptosis and necrosis.

Immunohistochemistry (IHC) and immunofluorescence (IF)—Patient TMA and slides containing mouse bone sections (4 mm thick) were kept on heat block at 58°C for 1 h. They were then rehydrated in a sequential passage of solutions starting with xylene for 30 min, 100% ethanol for 15 min, 95%, 90%, 80%, 75%, 50%, and 20% ethanol for 5 min each followed by immersion in double distilled water for 10 min. Antigen retrieval was performed by heat induced epitope retrieval at 95°C using Dako antigen retrieval solution (pH6). The antigen unmasking solution was first preheated at a high temperature in the microwave until boiling and then the slides were immersed into it and heated in a 95°C water bath for 30 min. Following this, the slides were gradually allowed to cool to room temperature and washed with double distilled water. For IHC only, slides were next immersed in 3% hydrogen peroxide (H_2O_2) in methanol for 10 min at room temperature. Slides were then blocked with 1% BSA+0.2% saponin in TBST at 4°C for 1 h and incubated overnight with primary antibody in the blocking buffer at 4°C. Biotinylated secondary antibodies (IHC) or fluorophore-conjugated secondary antibody (IF) were added. For IHC staining, slides were next washed with TBST and then incubated with avidin–biotin complex (Reagent A and Reagent B) for 30 min at room temperature, following the manufacturer's instructions. Next, diaminobenzidine solution (ImmPACT DAB) was added as a substrate for peroxidase until the desired staining intensity was developed. Hematoxylin was used to counter staining. Slides were dehydrated by gradual passage of slides from double distilled water to xylene in a reverse order mentioned earlier for rehydration of slides and mounted with Permount and covered with glass cover slips. The whole slides were next digitally scanned at Tissue Science Facility, UNMC. For IF, following incubation with secondary antibody cells were washed and mounted with Vectashield mounting media containing DAPI (Vector Laboratories, H1200) and photomicrographs were captured using confocal microscope. Images were processed using Ventana image viewer and ImageScope Viewer (for IHC) and Zen software (for IF). Quantification was performed based on number of ki67 positive/cleaved caspase-3 positive tumor cells compared to total number of tumor cells in

each zone using ImageJ Immunohistochemistry (IHC) Image Analysis Toolbox plugin and was validated by pathologist, Dr. Michael Muders. Graphical illustrations were made using GraphPad Prism 8 software.

Co-culture experiment—For NE-NE and NE-adeno co-culture experiments, DKD cells were cultured in 6-well plate, transfected with Scr or siNRP2 and incubated for 12h. DKD (NE-NE co-culture) or C4–2 (NE-adeno co-culture) cells were cultured separately on the coverslips without any transfection. The coverslips with either DKD or C4–2 cells were then placed into the 6-well chambers of transfected DKD cells. For adeno-adeno co-culture experiment, C4–2B cells were cultured in 6-well plate, transfected with Scr or siNRP2 and incubated for 12h. Coverslips with separately cultured C4–2 cells was then added into the 6-well chambers with transfected C4–2B cells. 48hr post transfection immunocytochemistry was performed for p-AKT and observed under confocal microscopy. For cell death assessment, after 12h of coverslip transfer, cells were treated with Docetaxel for 24h, PI staining was performed and observed under confocal microscopy. Co-culture experiment with VAMP2 +/− condition was performed in the similar way described above.

Immunocytochemistry—The cells were grown on the coverslips and after treatment, were washed with PBS and fixed in 4% paraformaldehyde solution. Cells were blocked with 3% BSA+0.2% saponin in TBST at 4°C for 1 h, followed by overnight incubation in primary antibody at 4°C. Next, fluorophore-conjugated secondary antibody was added for 60min and cells were co-immunostained with WGA or Phalloidin for 15 min. Coverslips were washed, mounted onto the glass slides using VECTASHIELD mounting medium with DAPI and photomicrographs were captured using confocal microscope.

Confocal microscopy—All the confocal images were captured in Zeiss LSM 800 Confocal Laser Scanning Microscope equipped with 4 lasers located in the UNMC confocal core facility, and images were analyzed using Zeiss Zen 2010 software. All confocal data was quantified using ImageJ software and graphical illustrations were prepared using GraphPad Prism 8 software.

Co-localization calculation—Co-localization of pAKT and VAMP2 with plasma membrane, either stained with phalloidin or wheat germ agglutinin (WGA), was quantified using Fiji ImageJ software with Coloc2 plugin. Costes p-values were calculated for each experiment.

RNA sequencing—RNA-seq was carried out for C4–2, DKD, C4–2B, C4–2B-ER, DKD-Scr and DKD-SiNRP2 in triplicate samples. RNA was isolated from the cells using the RNeasy Mini Kit (Qiagen, Germantown, MD) and RNA integrity quality was confirmed using the Agilent Bioanalyzer. A paired end read (2× 50 bp) sequencing run of RNA libraries were carried out with Illumina NextSeq 500. Sequences were aligned to human reference genome hg38. Data analysis was performed with the help of the Bioinformatics Core at UNMC. RNA abundance was estimated with feature Counts from the Sub-read package version 1.6.3. Downstream analyses were performed with the DESEQ2 R package version 1.18.1. A Principal component analysis (PCA) was performed using https://biit.cs.ut.ee/clustvis/. Differentially expressed genes (DEGs) were identified by pairwise

comparisons with the DESEQ2 package (v.1.12.3). Genes were retained as differentially expressed when the fold-change (FC) was >2 or < −2.

Mass spectrometry analysis—Mass Spectrometry was carried out on C4–2B, DKD Scr and DKD SiNRP2 cells. Cells were grown in 6-well plate in two different condition - control and knockdown of NRP2. Cells were transfected and grown in serum free RPMI media for 48hrs. After 48hrs, cell supernatant/conditioned media (CM) was collected (~2mL), cell debris were removed by centrifuging CM @3000g for 30-min. RPMI media only was used for background correction. Proteins were purified by acetone precipitation to remove vitamins, cholines and other small molecules contaminants. Mass Spectrometry analysis was carried out through LC-MS/MS using Thermo Q-Exactive-HF mass spectrometer and a nano RSLC Ultimate 3000 from Dionex. Spectra was processed using Mascot (Matrix Science, London, UK; version 2.6.1) and were subjected to a cutoff of 1% false discovery rate. Spectra was processed by MODIRO ver.1.1 (Protagen, Germany) software (from Proteomics & Metabolomics Facility of the Nebraska Center for Biotechnology at University of Nebraska, Lincoln).

Cytokine assay—Presence of cytokines in the CM of DKD and C4–2B Scr vs. siNRP2 cells was detected using human XL cytokine array kit following manufacturer's protocol. CM from the transfected cells was collected, centrifuged@3000g for 15-min, and stored at −80°C until further use. Assay membranes containing 105 different capture antibodies was blocked for 60min followed by overnight incubation in CM at 4°C. On the following day, the membranes were washed thrice (10min each), incubated with detection antibody cocktail for 60min, washed thrice (10min each) and incubated in streptavidin-HRP solution for 30min. The membranes were then washed thrice (10min each) and developed with chemiluminescent detection reagent using an X-ray film developer and cytokines spots were identified using transparency overlay template.

Bioinformatics—Gene Set Enrichment Analysis (GSEA) and pathway analysis using RNA-seq data of the above patient cohorts and the developed NE-like cells were performed using GSEA Software and Molecular Signature Database (MSigDB) (Subramanian et al., 2005), and DAVID bioinformatics resources 6.8 (Huang Da et al., 2009b) and (Huang Da et al., 2009a). Pathway analysis of the enriched proteomes after mass spectrometric analysis was done using g:Profiler (Raudvere et al., 2019). The RNA-seq data was downloaded from NCBI GEO using SRAtoolKit (url: https://trace.ncbi.nlm.nih.gov/Traces/sra/sra.cgi?view=software). The reads were aligned to mm10 with STAR (v.2.5.3a) and gene counts quantified with HTSeq (v.0.9.1). The raw counts were processed and normalized in DESeq2. Heatmap of normalized gene expression were generated using Heatmapper (Babicki et al., 2016). For the single cell RNA-seq analysis, the molecule_info.h5 files were downloaded from NCBI GEO (GSE151426). The matrix.h5 files were generated from molecule_info.h5 file using cellranger aggr software (10x Genomics) (Zheng et al., 2017). The matrix.h5 files for each sample were read into R using Seurat package (V4). The data was normalized, and doublet cells were removed. Cell type annotation was performed using SingleR (Aran et al., 2019) with mouse reference from Immunological Genome Project (ImmGen) (Heng et al., 2008). Mean difference between the groups were estimated using Student's t-test.

QUANTIFICATION AND STATISTICAL ANALYSIS

All the graphical illustrations and statistical tests were performed using GraphPad Prism 8 software (GraphPad software, Inc.). All data reported in graphs are expressed as mean ± standard error of mean (SEM), unless otherwise mentioned and were compared using standard two-tailed unpaired t test, unless otherwise mentioned. p values were considered statistically significant when less than 0.05. All experiments were repeated at least 3 times unless specified.

Supplementary Material

Refer to Web version on PubMed Central for supplementary material.

ACKNOWLEDGMENTS

The authors are grateful to the members of the Advanced Microscopy and Histology core of UNMC. The authors are also thankful for the sincere support received from Prostate Cancer Biorepository Network. Funding. Grant support was received by S.D. (1R21CA241234–01, NE-LB506, Lageschulte Fund) and K.D. (R01CA182435, R01CA239343, DOD W81XWH2110628).

REFERENCES

Abida W, Cyrta J, Heller G, Prandi D, Armenia J, Coleman I, Cieslik M, Benelli M, Robinson D, Van Allen EM, et al. (2019). Genomic correlates of clinical outcome in advanced prostate cancer. Proc. Natl. Acad. Sci. USA 116, 11428–11436. [PubMed: 31061129]

Aggarwal R, Huang J, Alumkal JJ, Zhang L, Feng FY, Thomas GV, Weinstein AS, Friedl V, Zhang C, Witte ON, et al. (2018). Clinical and genomic characterization of treatment-emergent small-cell neuroendocrine prostate cancer: a multi-institutional prospective study. J. Clin. Oncol 36, 2492–2503. [PubMed: 29985747]

Akamatsu S, Inoue T, Ogawa O, and Gleave ME (2018). Clinical and molecular features of treatment-related neuroendocrine prostate cancer. Int. J. Urol 25, 345–351. [PubMed: 29396873]

Aparicio A, Logothetis CJ, and Maity SN (2011). Understanding the lethal variant of prostate cancer: power of examining extremes. Cancer Discov. 1, 466–468. [PubMed: 22586648]

Aparicio AM, Harzstark AL, Corn PG, Wen S, Araujo JC, Tu SM, Pagliaro LC, Kim J, Millikan RE, Ryan C, et al. (2013). Platinum-based chemotherapy for variant castrate-resistant prostate cancer. Clin. Cancer Res 19, 3621–3630. [PubMed: 23649003]

Aran D, Looney AP, Liu L, Wu E, Fong V, Hsu A, Chak S, Naikawadi RP, Wolters PJ, Abate AR, et al. (2019). Reference-based analysis of lung single-cell sequencing reveals a transitional profibrotic macrophage. Nat. Immunol 20, 163–172. [PubMed: 30643263]

Babicki S, Arndt D, Marcu A, Liang Y, Grant JR, Maciejewski A, and Wishart DS (2016). Heatmapper: web-enabled heat mapping for all. Nucleic Acids Res 44, W147–W153. [PubMed: 27190236]

Bakouny Z, and Choueiri TK (2020). IL-8 and cancer prognosis on immunotherapy. Nat. Med 26, 650–651. [PubMed: 32405061]

Beltran H, Rickman DS, Park K, Chae SS, Sboner A, Macdonald TY, Wang Y, Sheikh KL, Terry S, Tagawa ST, et al. (2011). Molecular characterization of neuroendocrine prostate cancer and identification of new drug targets. Cancer Discov. 1, 487–495. [PubMed: 22389870]

Beltran H, Prandi D, Mosquera JM, Benelli M, Puca L, Cyrta J, Marotz C, Giannopoulou E, Chakravarthi BV, Varambally S, et al. (2016). Divergent clonal evolution of castration-resistant neuroendocrine prostate cancer. Nat. Med 22, 298–305. [PubMed: 26855148]

Benten D, Behrang Y, Unrau L, Weissmann V, Wolters-Eisfeld G, Burdak-Rothkamm S, Stahl FR, Anlauf M, Grabowski P, Mobs M, et al. (2018). Establishment of the first well-differentiated

human pancreatic neuroendocrine tumor model. Mol. Cancer Res 16, 496–507. [PubMed: 29330294]

Bloom O, Evergren E, Tomilin N, Kjaerulff O, Low P, Brodin L, Pieribone VA, Greengard P, and Shupliakov O (2003). Colocalization of synapsin and actin during synaptic vesicle recycling. J. Cell Biol 161, 737–747. [PubMed: 12756235]

Borkowetz A, Froehner M, Rauner M, Conrad S, Erdmann K, Mayr T, Datta K, Hofbauer LC, Baretton GB, Wirth M, et al. (2020). Neuropilin-2 is an independent prognostic factor for shorter cancer-specific survival in patients with acinar adenocarcinoma of the prostate. Int. J. Cancer 146, 2619–2627. [PubMed: 31509606]

Brady NJ, Bagadion AM, Singh R, Conteduca V, Van Emmenis L, Arceci E, Pakula H, Carelli R, Khani F, Bakht M, et al. (2021). Temporal evolution of cellular heterogeneity during the progression to advanced AR-negative prostate cancer. Nat. Commun 12, 3372. [PubMed: 34099734]

Butler W, and Huang J (2021). Neuroendocrine cells of the prostate: Histology, biological functions, and molecular mechanisms. Precis. Clin. Med 4, 25–34. [PubMed: 33842835]

Chenouard N, Xuan F, and Tsien RW (2020). Synaptic vesicle traffic is supported by transient actin filaments and regulated by PKA and NO. Nat. Commun 11, 5318. [PubMed: 33087709]

Cives M, Pelle E, Quaresmini D, Rizzo FM, Tucci M, and Silvestris F (2019). The tumor microenvironment in neuroendocrine tumors: Biology and therapeutic implications. Neuroendocrinology 109, 83–99. [PubMed: 30699437]

Conteduca V, Oromendia C, Eng KW, Bareja R, Sigouros M, Molina A, Faltas BM, Sboner A, Mosquera JM, Elemento O, et al. (2019). Clinical features of neuroendocrine prostate cancer. Eur. J. Cancer 121, 7–18. [PubMed: 31525487]

Dutta S, Roy S, Polavaram NS, Baretton GB, Muders MH, Batra S, and Datta K (2016a). NRP2 transcriptionally regulates its downstream effector WDFY1. Sci. Rep 6, 23588. [PubMed: 27026195]

Dutta S, Roy S, POLavaram NS, Stanton MJ, Zhang H, Bhola T, Honscheid P, Donohue TM Jr., Band H, Batra SK, et al. (2016b). Neuropilin-2 regulates endosome maturation and EGFR trafficking to support cancer cell pathobiology. Cancer Res. 76, 418–428. [PubMed: 26560516]

Flechon A, Pouessel D, Ferlay C, Perol D, Beuzeboc P, Gravis G, Joly F, Oudard S, Deplanque G, Zanetta S, et al. (2011). Phase II study of carboplatin and etoposide in patients with anaplastic progressive metastatic castration-resistant prostate cancer (mCRPC) with or without neuroendocrine differentiation: results of the French Genito-Urinary Tumor Group (GETUG) P01 trial. Ann. Oncol 22, 2476–2481. [PubMed: 21436186]

Gilder AS, Natali L, Van Dyk DM, Zalfa C, Banki MA, Pizzo DP, Wang H, Klemke RL, Mantuano E, and Gonias SL (2018). The urokinase receptor induces a mesenchymal gene expression signature in glioblastoma cells and promotes tumor cell survival in neurospheres. Sci. Rep 8, 2982. [PubMed: 29445239]

Guan G, Niu X, Qiao X, Wang X, Liu J, and Zhong M (2020). Upregulation of neural cell adhesion molecule 1 (NCAM1) by hsa-miR-141–3p suppresses ameloblastoma cell migration. Med. Sci. Monit 26, e923491. [PubMed: 32269209]

Guo H, Ci X, Ahmed M, Hua JT, Soares F, Lin D, Puca L, Vosoughi A, Xue H, Li E, et al. (2019). ONECUT2 is a driver of neuroendocrine prostate cancer. Nat. Commun 10, 278. [PubMed: 30655535]

Heng TS, Painter MW, and Immunological genome project C. (2008). The Immunological Genome Project: networks of gene expression in immune cells. Nat. Immunol 9, 1091–1094. [PubMed: 18800157]

Huang J, Yao JL, Zhang L, Bourne PA, Quinn AM, di Sant'Agnese PA, and Reeder JE (2005). Differential expression of interleukin-8 and its receptors in the neuroendocrine and non-neuroendocrine compartments of prostate cancer. Am. J. Pathol 166, 1807–1815. [PubMed: 15920165]

Huang Da W, Sherman BT, and Lempicki RA (2009a). Bioinformatics enrichment tools: paths toward the comprehensive functional analysis of large gene lists. Nucleic Acids Res. 37, 1–13. [PubMed: 19033363]

Huang Da W, Sherman BT, and Lempicki RA (2009b). Systematic and integrative analysis of large gene lists using DAVID bioinformatics resources. Nat. Protoc 4, 44–57. [PubMed: 19131956]

Huang B, Gao Y, Tian D, and Zheng M (2010). A small interfering ABCE1-targeting RNA inhibits the proliferation and invasiveness of small cell lung cancer. Int. J. Mol. Med 25, 687–693. [PubMed: 20372810]

Inoue K, Slaton JW, Eve BY, Kim SJ, Perrotte P, Balbay MD, Yano S, Bar-Eli M, Radinsky R, Pettaway CA, and Dinney CP (2000). Interleukin 8 expression regulates tumorigenicity and metastases in androgen-independent prostate cancer. Clin. Cancer Res 6, 2104–2119. [PubMed: 10815938]

Jin RJ, Wang Y, Masumori N, Ishii K, Tsukamoto T, Shappell SB, Hayward SW, Kasper S, and Matusik RJ (2004). NE-10 neuroendocrine cancer promotes the LNCaP xenograft growth in castrated mice. Cancer Res. 64, 5489–5495. [PubMed: 15289359]

Jolly MK, Kulkarni P, Weninger K, Orban J, and Levine H (2018). Phenotypic plasticity, bet-hedging, and androgen independence in prostate cancer: role of non-genetic heterogeneity. Front. Oncol 8, 50. [PubMed: 29560343]

Kara G, Tuncer S, Turk M, and Denkbas EB (2015). Downregulation of ABCE1 via siRNA affects the sensitivity of A549 cells against chemotherapeutic agents. Med. Oncol 32, 103. [PubMed: 25744244]

Kersemans V, Cornelissen B, Allen PD, Beech JS, and Smart SC (2013). Subcutaneous tumor volume measurement in the awake, manually restrained mouse using MRI. J. Magn. Reson. Imaging 37, 1499–1504. [PubMed: 23023925]

Koch AE, Polverini PJ, Kunkel SL, Harlow LA, Dipietro LA, Elner VM, Elner SG, and Strieter RM (1992). Interleukin-8 as a macrophage-derived mediator of angiogenesis. Science 258, 1798–1801. [PubMed: 1281554]

Ku SY, Rosario S, Wang Y, Mu P, Seshadri M, Goodrich ZW, Goodrich MM, Labbe DP, Gomez EC, Wang J, et al. (2017). Rb1 and Trp53 cooperate to suppress prostate cancer lineage plasticity, metastasis, and anti-androgen resistance. Science 355, 78–83. [PubMed: 28059767]

Labrecque MP, Coleman IM, Brown LG, True LD, Kollath L, Lakely B, Nguyen HM, Yang YC, da Costa RMG, Kaipainen A, et al. (2019). Molecular profiling stratifies diverse phenotypes of treatment-refractory metastatic castration-resistant prostate cancer. J. Clin. Invest 129, 4492–4505. [PubMed: 31361600]

Laskaratos FM, Levi A, Schwach G, Pfragner R, Hall A, Xia D, von Stempel C, Bretherton J, Thanapirom K, Alexander S, et al. (2021). Transcriptomic profiling of in vitro tumor-stromal cell paracrine crosstalk identifies involvement of the integrin signaling pathway in the pathogenesis of mesenteric fibrosis in human small intestinal neuroendocrine neoplasms. Front. Oncol 11, 629665. [PubMed: 33718208]

Li Y, He Y, Butler W, Xu L, Chang Y, Lei K, Zhang H, Zhou Y, Gao AC, Zhang Q, et al. (2019). Targeting cellular heterogeneity with CXCR2 blockade for the treatment of therapy-resistant prostate cancer. Sci. Transl. Med 11.

Li Y, Zhang B, Xiang L, Xia S, Kucuk O, Deng X, Boise LH, and Dong JT (2020). TGF-Beta causes docetaxel resistance in prostate cancer via the induction of Bcl-2 by acetylated KLF5 and protein stabilization. Theranostics 10, 7656–7670. [PubMed: 32685011]

Liang Y, Ma C, LI F, Nie G, and Zhang H (2020). The role of contactin 1 in cancers: what we know so far. Front. Oncol 10, 574208. [PubMed: 33194679]

Lin Y, Fukuchi J, Hiipakka RA, Kokontis JM, and Xiang J (2007). Upregulation of Bcl-2 is required for the progression of prostate cancer cells from an androgen-dependent to an androgen-independent growth stage. Cell Res. 17, 531–536. [PubMed: 17404601]

Liu D, Kuai Y, Zhu R, Zhou C, Tao Y, Han W, and Chen Q (2020). Prognosis of prostate cancer and bone metastasis pattern of patients: a SEER-based study and a local hospital based study from China. Sci. Rep 10, 9104. [PubMed: 32499554]

Mu P, Zhang Z, Benelli M, Karthaus WR, Hoover E, Chen CC, Wongvipat J, Ku SY, Gao D, Cao Z, et al. (2017). SOX2 promotes lineage plasticity and antiandrogen resistance in TP53- and RB1-deficient prostate cancer. Science 355, 84–88. [PubMed: 28059768]

Nadal R, Schweizer M, Kryvenko ON, Epstein JI, and Eisenberger MA (2014). Small cell carcinoma of the prostate. Nat. Rev. Urol 11, 213–219. [PubMed: 24535589]

Orlando M, Lignani G, Maragliano L, Fassio A, Onofri F, Baldelli P, Giovedi S, and Benfenati F (2014). Functional role of ATP binding to synapsin I in synaptic vesicle trafficking and release dynamics. J. Neurosci 34, 14752–14768. [PubMed: 25355227]

Patel GK, Chugh N, and Tripathi M (2019). Neuroendocrine differentiation of prostate cancer-an intriguing example of tumor evolution at play. Cancers 11, 1405.

Quintanal-Villalonga A, Chan JM, Yu HA, Pe'er D, Sawyers CL, Sen T, and Rudin CM (2020). Lineage plasticity in cancer: a shared pathway of therapeutic resistance. Nat. Rev. Clin. Oncol 17, 360–371. [PubMed: 32152485]

Rathore M, Girard C, Ohanna M, Tichet M, Ben Jouira R, Garcia E, Larbret F, Gesson M, Audebert S, Lacour JP, et al. (2019). Cancer cell-derived long pentraxin 3 (PTX3) promotes melanoma migration through a toll-like receptor 4 (TLR4)/NF-kappaB signaling pathway. Oncogene 38, 5873–5889. [PubMed: 31253871]

Raudvere U, Kolberg L, Kuzmin I, Arak T, Adler P, Peterson H, and Vilo J (2019). g:Profiler: a web server for functional enrichment analysis and conversions of gene lists (2019 update). Nucleic Acids Res. 47, W191–W198. [PubMed: 31066453]

Rindi G, and Wiedenmann B (2020). Neuroendocrine neoplasia of the gastrointestinal tract revisited: towards precision medicine. Nat. Rev. Endocrinol 16, 590–607. [PubMed: 32839579]

Roy S, BAG AK, Dutta S, Polavaram NS, Islam R, Schellenburg S, Banwait J, Guda C, Ran S, Hollingsworth MA, et al. (2018). Macrophage-Derived neuropilin-2 exhibits novel tumor-promoting functions. Cancer Res. 78, 5600–5617. [PubMed: 30111533]

Sang M, Hulsurkar M, Zhang X, Song H, Zheng D, Zhang Y, Li M, Xu J, Zhang S, Ittmann M, and Li W (2016). GRK3 is a direct target of CREB activation and regulates neuroendocrine differentiation of prostate cancer cells. Oncotarget 7, 45171–45185. [PubMed: 27191986]

Schulz A, Gorodetska I, Behrendt R, Fuessel S, Erdmann K, Foerster S, Datta K, Mayr T, Dubrovska A, and Muders MH (2019). Linking NRP2 with EMT and chemoradioresistance in bladder cancer. Front. Oncol 9, 1461. [PubMed: 32038994]

Shiota M, Fujimoto N, Matsumoto T, Tsukahara S, Nagakawa S, Ueda S, Ushijima M, Kashiwagi E, Takeuchi A, Inokuchi J, et al. (2021). Differential impact of TGFB1 variation by metastatic status in androgen-deprivation therapy for prostate cancer. Front. Oncol 11, 697955. [PubMed: 34113577]

Smith MR, Saad F, Chowdhury S, Oudard S, Hadaschik BA, Graff JN, Olmos D, Mainwaring PN, Lee JY, Uemura H, et al. (2018). Apalutamide treatment and metastasis-free survival in prostate cancer. N. Engl. J. Med 378, 1408–1418. [PubMed: 29420164]

Somasundaram A, and Taraska JW (2018). Local protein dynamics during microvesicle exocytosis in neuroendocrine cells. Mol. Biol. Cell 29, 1891–1903. [PubMed: 29874123]

Stanton MJ, Dutta S, Zhang H, Polavaram NS, Leontovich AA, Honscheid P, Sinicrope FA, Tindall DJ, Muders MH, and Datta K (2013). Autophagy control by the VEGF-C/NRP-2 axis in cancer and its implication for treatment resistance. Cancer Res. 73, 160–171. [PubMed: 23149913]

Subramanian A, Tamayo P, Mootha VK, Mukherjee S, Ebert BL, Gillette MA, Paulovich A, Pomeroy SL, Golub TR, Lander ES, and Mesirov JP (2005). Gene set enrichment analysis: a knowledge-based approach for interpreting genome-wide expression profiles. Proc. Natl. Acad. Sci. USA 102, 15545–15550. [PubMed: 16199517]

Tritschler S, Erdelkamp R, Stief C, and Hentrich M (2017). [Neuroendocrine prostate cancer]. Urologe A 56, 1475–1484. [PubMed: 29063171]

Wang XD, Hu R, Ding Q, Savage TK, Huffman KE, Williams N, Cobb MH, Minna JD, Johnson JE, and Yu Y (2019). Subtype-specific secretomic characterization of pulmonary neuroendocrine tumor cells. Nat. Commun 10, 3201. [PubMed: 31324758]

Wiedenmann B, John M, Ahnert-Hilger G, and Riecken EO (1998). Molecular and cell biological aspects of neuroendocrine tumors of the gastroen-teropancreatic system. J. Mol. Med. (Berl) 76, 637–647. [PubMed: 9725766]

Wright ME, Tsai MJ, and Aebersold R (2003). Androgen receptor represses the neuroendocrine transdifferentiation process in prostate cancer cells. Mol. Endocrinol 17, 1726–1737. [PubMed: 12775765]

Xu X, Yu Y, Zong K, Lv P, and Gu Y (2019). Up-regulation of IGF2BP2 by multiple mechanisms in pancreatic cancer promotes cancer proliferation by activating the PI3K/Akt signaling pathway. J. Exp Clin. Cancer Res 38, 497. [PubMed: 31852504]

Zhan P, Ji YN, and Yu LK (2013). VEGF is associated with the poor survival of patients with prostate cancer: a meta-analysis. Transl. Androl. Urol 2, 99–105. [PubMed: 26816732]

Zhang Y, Zheng D, Zhou T, Song H, Hulsurkar M, Su N, Liu Y, Wang Z, Shao L, Ittmann M, et al. (2018). Androgen deprivation promotes neuroendocrine differentiation and angiogenesis through CREB-EZH2-TSP1 pathway in prostate cancers. Nat. Commun 9, 4080. [PubMed: 30287808]

Zheng GXY, Terry JM, Belgrader P, Ryvkin P, Bent ZW, Wilson R, Ziraldo SB, Wheeler TD, McDermott GP, Zhu J, et al. (2017). Massively parallel digital transcriptional profiling of single cells. Nat. Commun 8, 14049. [PubMed: 28091601]

Highlights

- NRP2 is highly expressed in NE-like prostate cancer
- NRP2 regulates the fusion of secretory vesicles to plasma membrane
- The secretion of several cytokines, including IL-8, is regulated by NRP2
- NRP2-depletion from NE-like cells sensitizes adjacent adenocarcinoma to chemotherapy

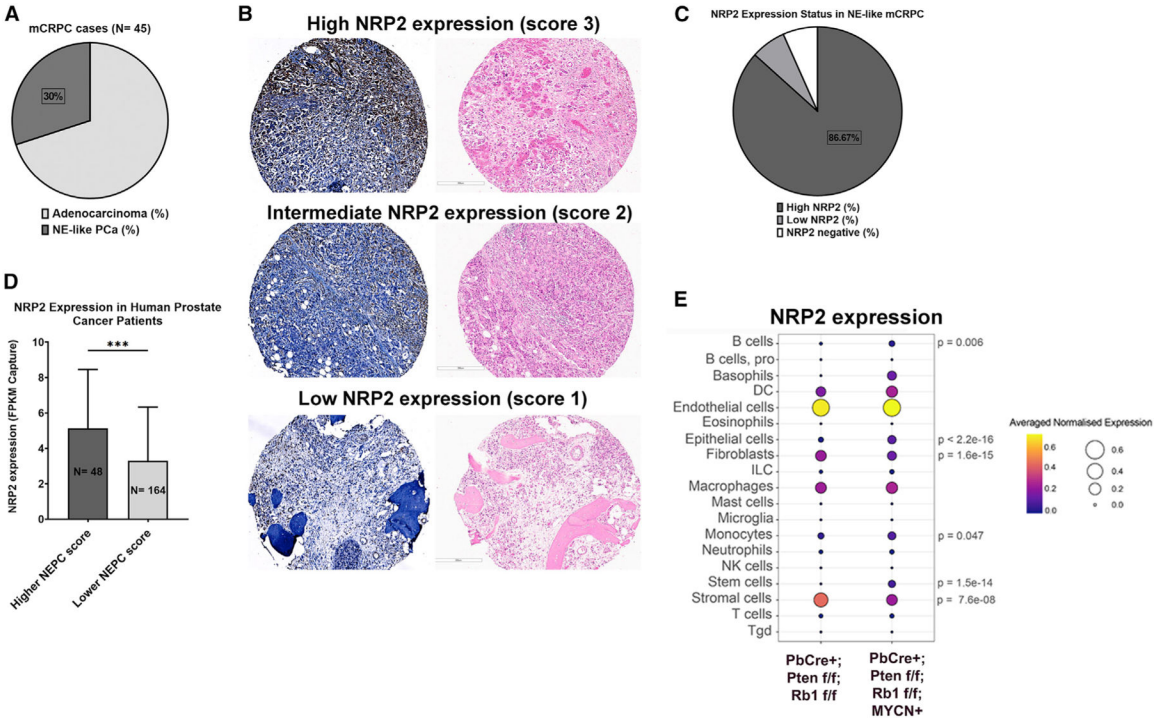

Figure 1. NRP2 is highly expressed in human NE-like PCa and AR-negative PCa mouse model

(A–C) Analysis of Prostate Cancer Biorepository Network (PCBN) mCRPC patient cohort (N = 45).

(A) Percentage of mCRPC patients with NE differentiation.

(B) Representative figures of high, intermediate, and low NRP2 expression in patient tissues coming from both visceral and bone metastatic cores.

(C) Percentage of patients having high NRP2 expression in NE-like mCRPC patients (IHC score 2 and 3).

(D) NRP2 expression in SU2C-PCF patient cohort.

(E) Single-cell RNA sequencing (RNA-seq) analysis of advanced AR-negative PCa mouse model (GSE151426) showing NRP2 expression. NEPC, NE PCa. Data represented as mean ± SEM.

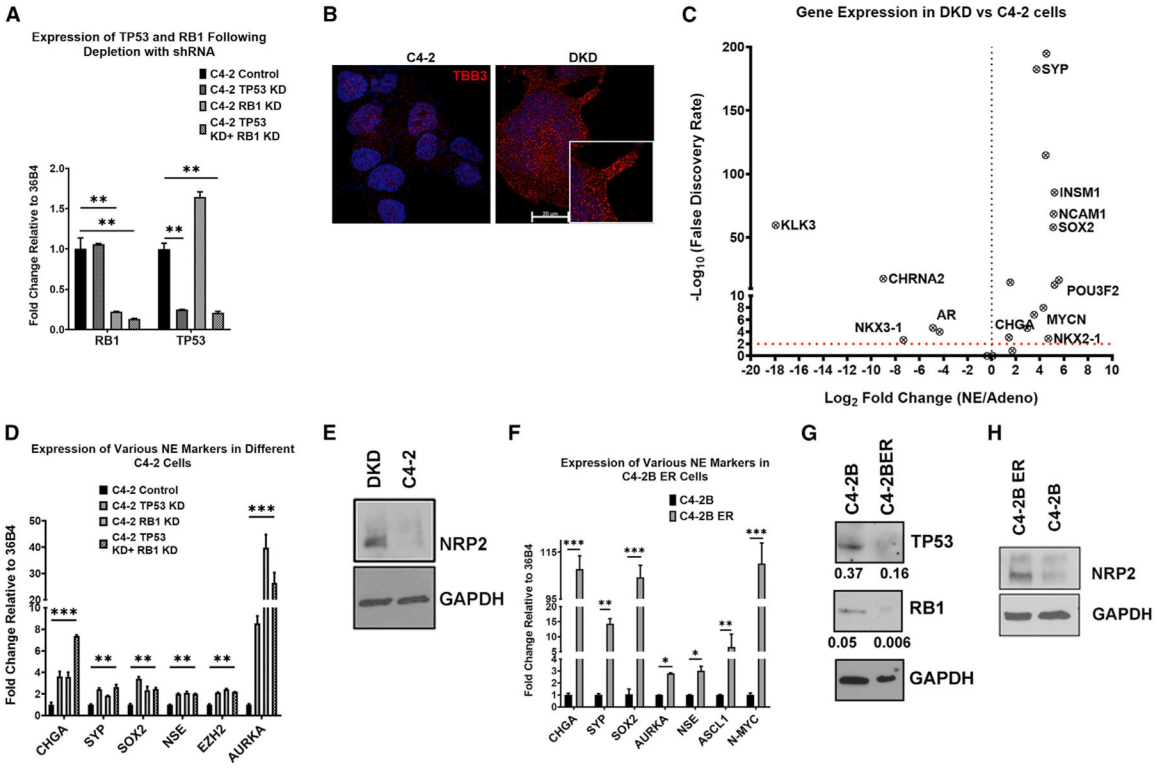

Figure 2. Characterization of NE-like PCa cells

(A–E) Characterization of C4–2 TP53 + RB1 double-knockdown (DKD) cell.

(A) *TP53* and *RB1* expression by real-time PCR.

(B) The appearance of long neurite-like branched processes in DKD cells shown by B3-tubulin staining (red).

(C) RNA-seq analysis of DKD and its syngeneic adenocarcinoma cells, C4–2.

(D) Real-time PCR of canonical NE markers.

(E) NRP2 expression in DKD cells compared with C4–2.

(F–H) Characterization of C4–2B enzalutamide-resistant (ER) cells. (F) Real-time PCR of canonical NE markers. (G) TP53 and RB1 protein expression in C4–2B ER cells compared with its syngeneic adenocarcinoma cells, C4–2B. The densitometric calculations are provided below each panel. (H) NRP2 expression in C4–2B ER cells compared with C4–2B. Data represented as mean ± SEM (n = 3).

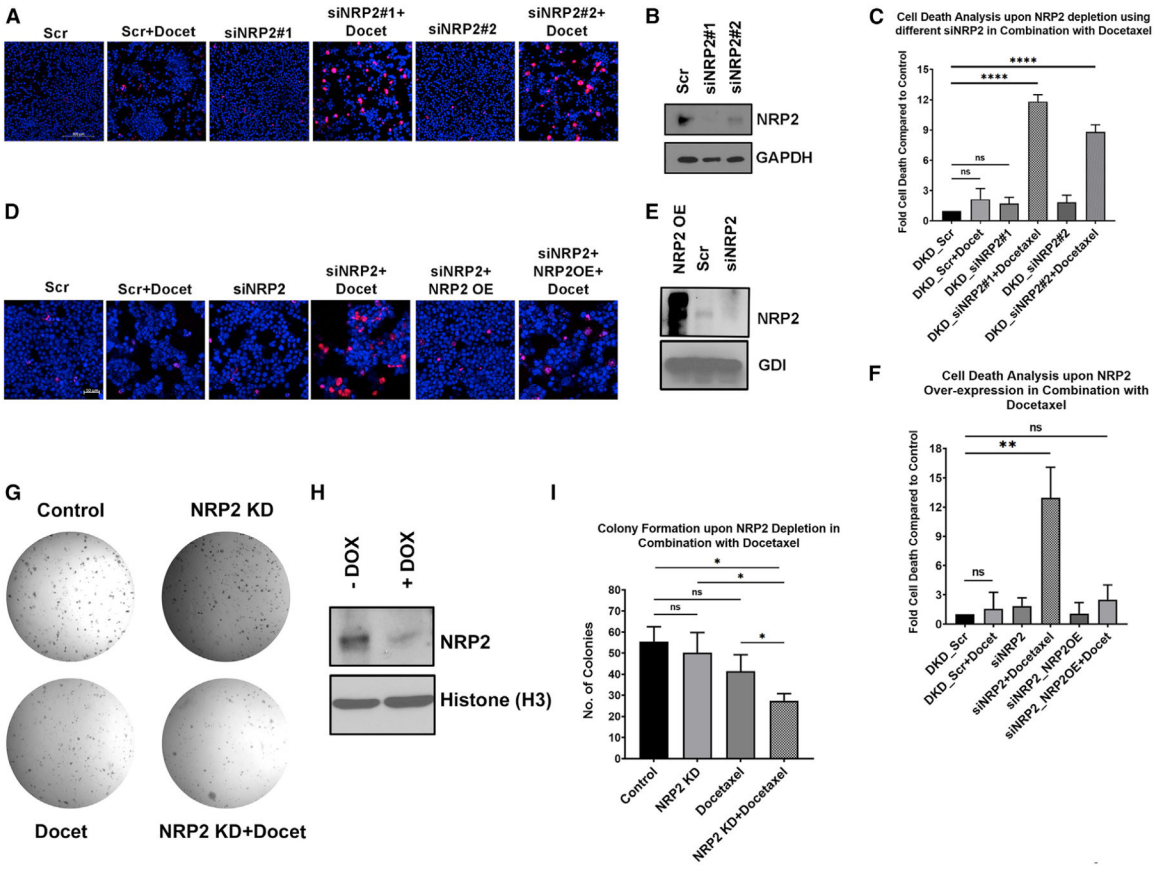

Figure 3. NRP2 depletion increases the efficacy of the front-line chemotherapeutic agents

(A) Effect of NRP2 knockdown on the efficacy of docetaxel by propidium iodide (PI; red)-based cell death analysis.

(B) Western blot showing the efficiency of different siRNAs to knock down NRP2.

(C) Quantitation of (A).

(D) Reversal of the chemo-sensitive phenotype of NRP2 knocked down NE-like (DKD) cells upon NRP2 overexpression by PI (red)-based cell death analysis.

(E) Western blot showing NRP2 overexpression.

(F) Quantitation of (D).

(G–I) DKD cells having stable shNRP2 expression upon Dox induction were used.

(G) Colony formation assay showing the effect of NRP2 depletion on the efficacy of docetaxel to inhibit the clonogenic potential of the cells.

(H) Western blot of Dox-inducible NRP2 knockdown.

(I) Quantitation of (G). OE, overexpression; DOX, doxycycline. Data represented as mean ± SEM (n = 3).

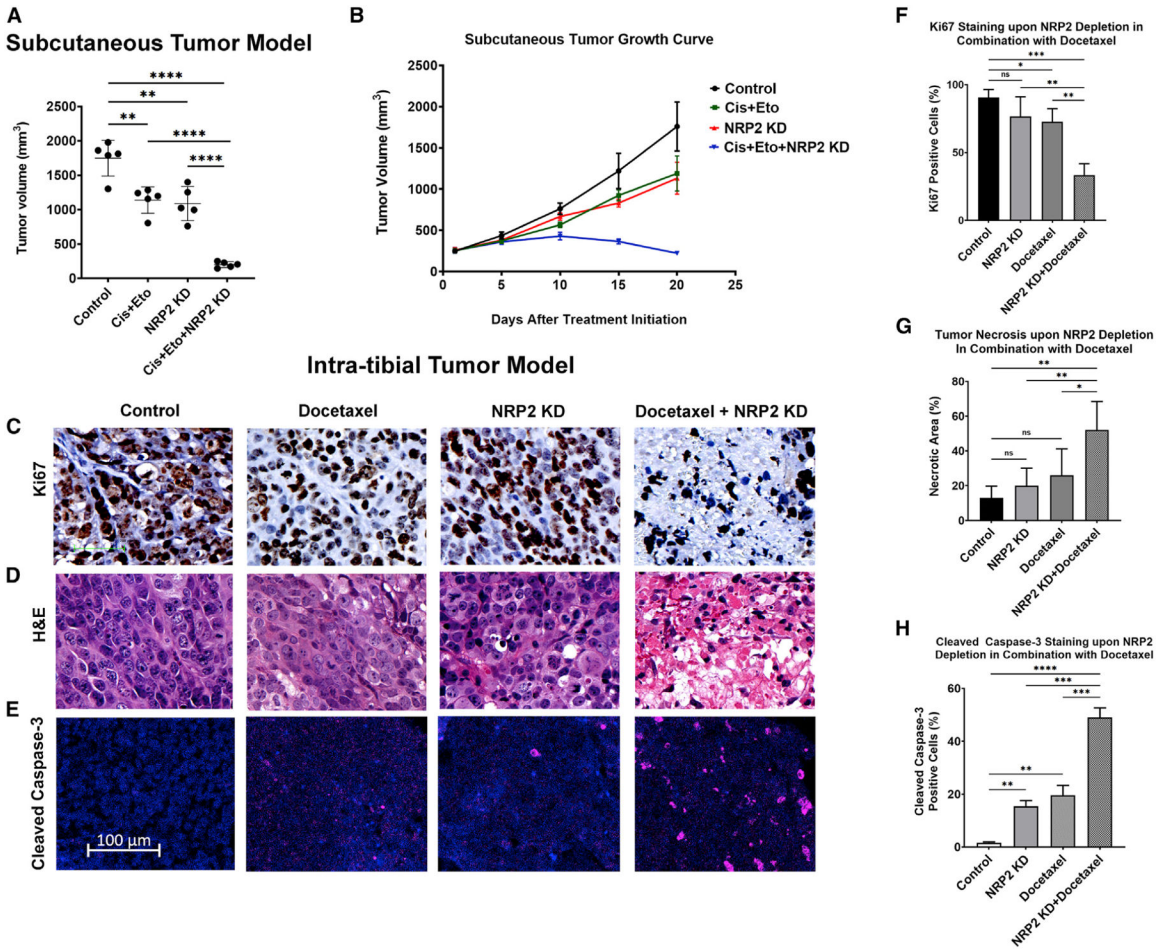

Figure 4. NRP2 depletion increases the efficacy of chemotherapy *in vivo*

(A and B) Effect of NRP2 depletion with or without cisplatin-etoposide (cis + eto) treatment in subcutaneous tumor model.

(A) Calculation of tumor volume in different treatment groups.

(B) Tumor growth curve over the period of treatment.

(C–H) Immunohistochemistry (IHC), immunofluorescence (IF), and H&E staining to evaluate cell proliferation, necrosis, and apoptosis upon NRP2 depletion with or without docetaxel treatment in intra-tibial tumor model.

(C) IHC of ki67.

(D) H&E staining.

(E) IF analysis of cleaved caspase-3 (purple).

(F) Quantitation of (C).

(G) Quantitation of (D).

(H). Quantitation of (E). Data represented as mean ± SEM.

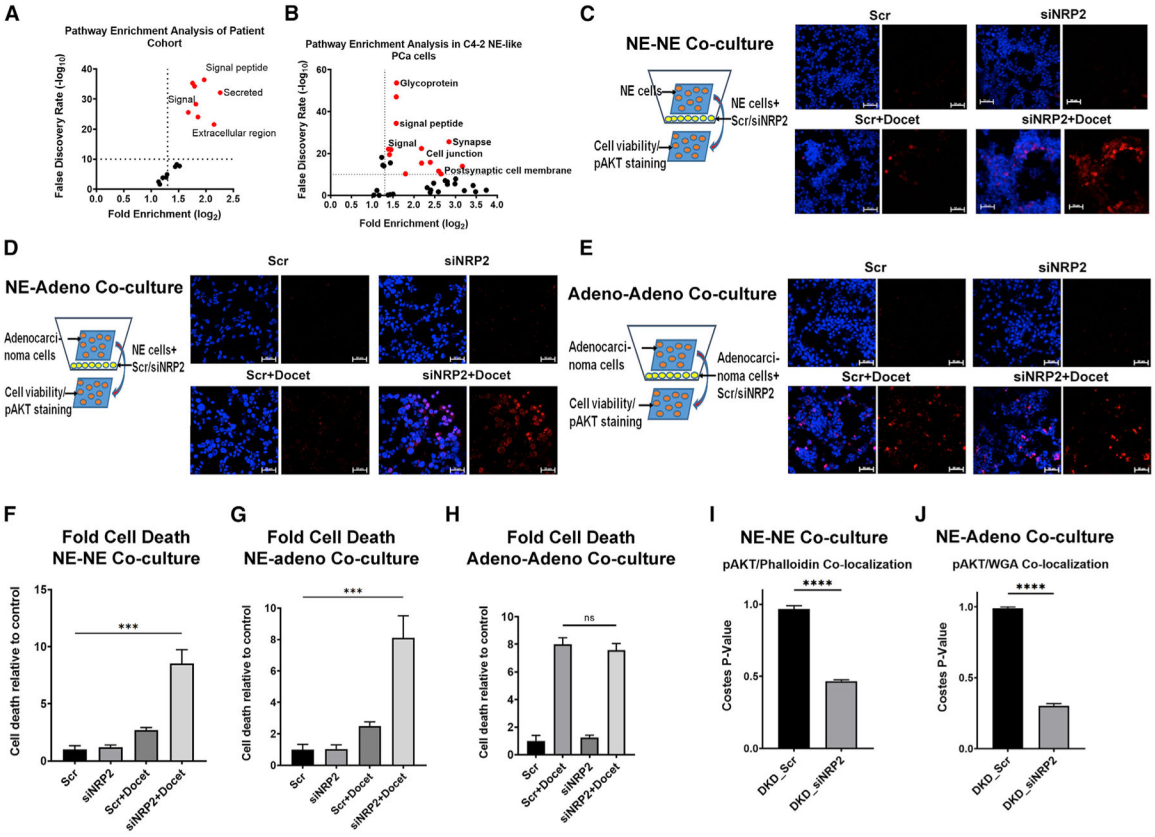

Figure 5. NRP2 confers chemo-resistance to the surrounding cancer cells in a paracrine manner

(A) Pathway analysis from the RNA-seq data of SU2C-PCF patient cohort. Graph showing enriched pathways in the NE-like PCa patients compared with adenocarcinoma.

(B) Pathway analysis from the RNA-seq data of DKD and C4–2 cells. Graph showing enriched pathways in the NE-like PCa cells (DKD) compared with adenocarcinoma cells (C4–2).

(C–H) PI (red)-based cell viability analysis of different co-culture assays as indicated.

(C) Cell viability of NE-like PCa (DKD) cells co-cultured with NRP2 +/− NE-like PCa (DKD) cells.

(D) Cell viability of adenocarcinoma (C4–2) cells co-cultured with NRP2 +/− NE-like PCa (DKD) cells.

(E) Cell viability of adenocarcinoma (C4–2) cells co-cultured with NRP2 +/− adenocarcinoma (C4–2B).

(F–H) Graphs showing fold change in cell death relative to control.

(F) Quantitation of (C).

(G) Quantitation of (D).

(H) Quantitation of (F).

(I) Quantitation of co-localization pAKT (Ser 473) staining with plasma membrane when NE-like PCa (DKD) cells were co-cultured with NRP2 +/− NE-like PCa (DKD) cells.

(J) Quantitation of co-localization pAKT (Ser 473) staining with plasma membrane when adenocarcinoma (C4–2) cells were co-cultured with NRP2 +/− NE-like PCa (DKD) cells. Data represented as mean ± SEM (n = 3).

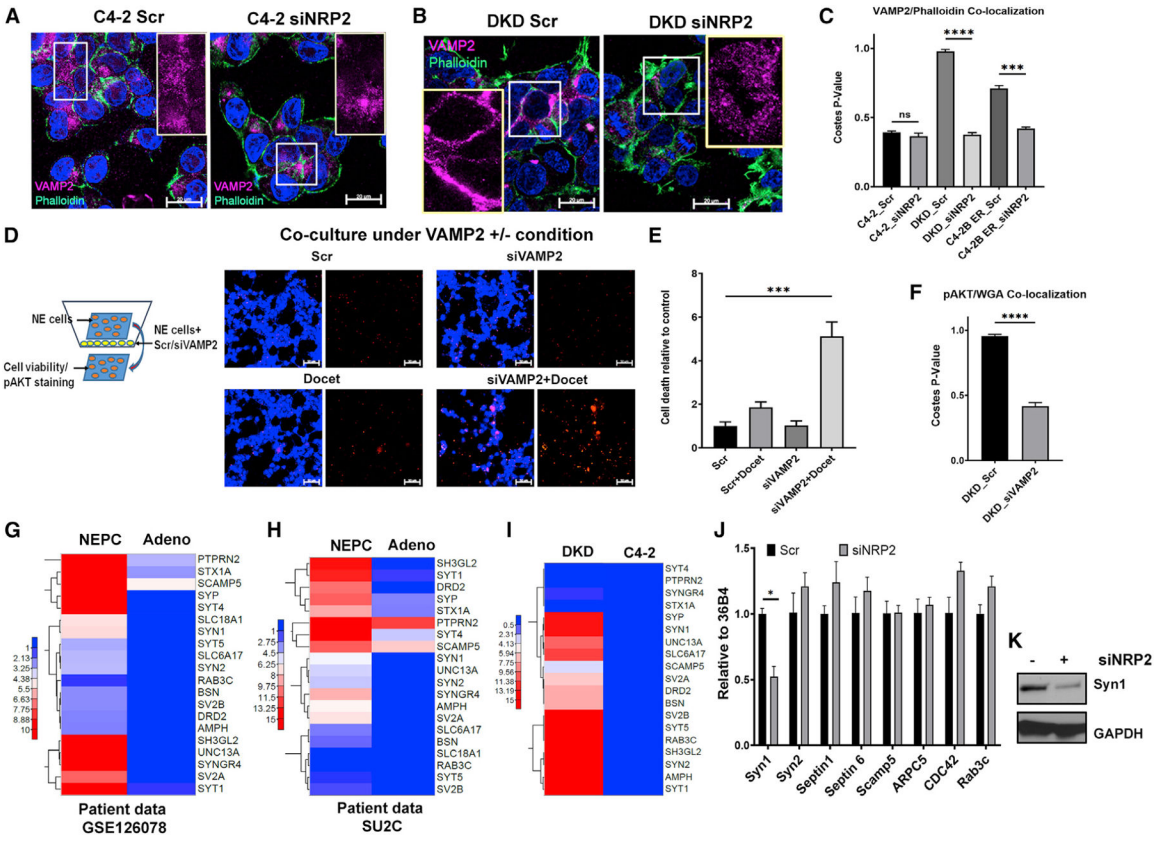

Figure 6. NRP2 regulates exocytosis in the NE-like PCa cells by controlling the vesicular fusion pathway

(A) VAMP2-positive vesicle localization (pink) in C4–2 cells under +/− NRP2 condition.

(B) VAMP2-positive vesicle localization (pink) in DKD cells under +/− NRP2 condition.

(C) Quantitation of (A) and (B).

(D) Cell viability of DKD cells co-cultured with VAMP2 +/− DKD cells (PI, red).

(E) Quantitation of (D).

(F) Quantitation of pAKT (Ser 473) (green) co-localization with plasma membrane in DKD cells co-cultured with VAMP2 +/− DKD cells.

(G) Differential gene expression in NE-like PCa patients compared with adenocarcinoma (GSE126078).

(H) Differential gene expression in NE-like PCa patients compared with adenocarcinoma (SU2C/PCF).

(I) Differential gene expression in DKD cells compared with C4–2.

(J) Real-time PCR of a set of genes identified in gene set enrichment analysis (GSEA).

(K) Western blot of Syn1 upon NRP2 knockdown. Data represented as mean ± SEM (n = 3).

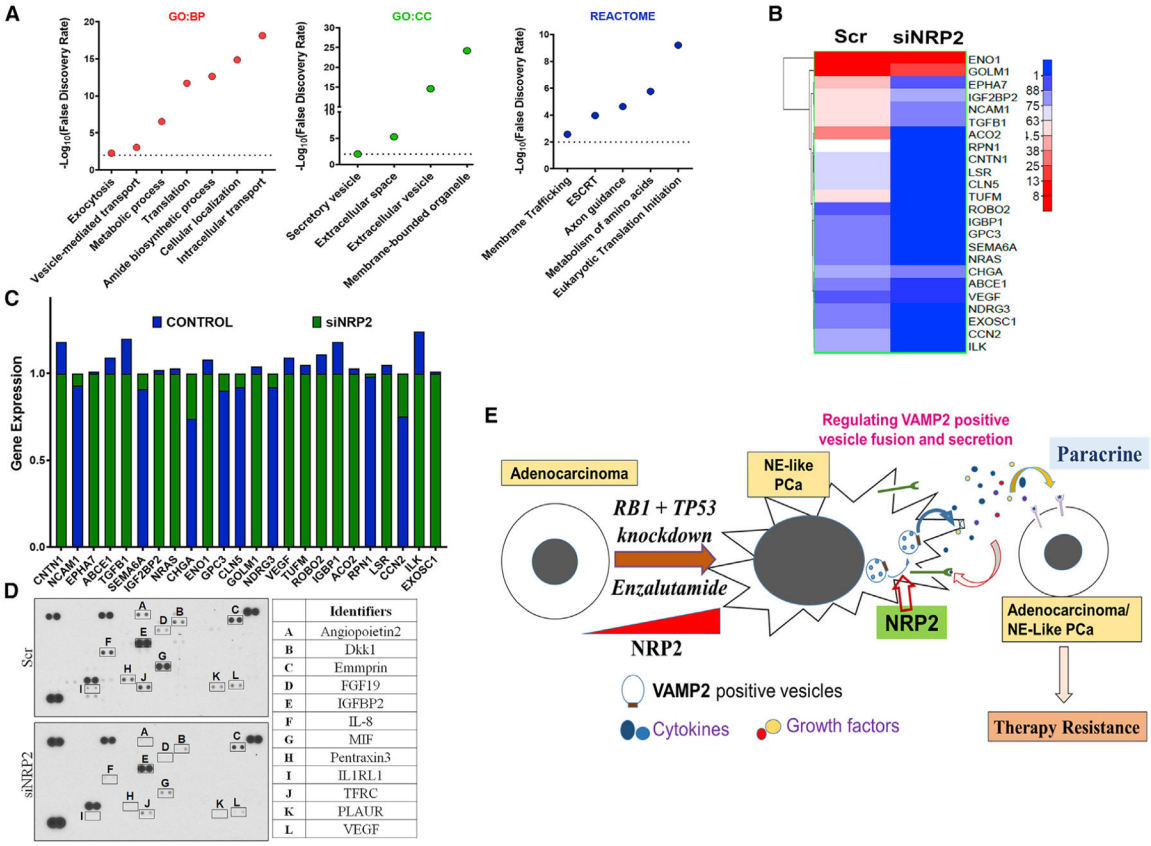

Figure 7. Characterization of NRP2-regulated secretome in NE-like PCa cells

(A) Pathway analysis of secretome enriched in the spent media of NE-like PCa cells (DKD).

(B) Effect of NRP2 knockdown on the secretome in DKD cells shown by mass spectrometric analysis.

(C) Gene expression of different proteins in the secretome in DKD cells with and without NRP2 depletion.

(D) Cytokine array using the spent media of DKD cells with and without NRP2 depletion.

(E) Schematic diagram showing NRP2's role in regulating secretory phenotype in NE-like PCa cells.

KEY RESOURCES TABLE

REAGENT or RESOURCE	SOURCE	IDENTIFIER
Antibodies		
NRP2 (Western Blotting)	R&D Systems	AF2215
NRP2 (IHC)	Atlas Antibodies,	HPA039980
AR	Cell Signaling	5153
TP53	Cell Signaling	2524
RB1	Cell Signaling	9309
SYP	Cell Signaling	36406
SOX2	Cell Signaling	23064
Synapsin-1	Cell Signaling	5297
IL-8	R&D Systems	MAB208
NKX3.1	Cell Signaling	83700
GAPDH	Cell Signaling	5174
Histone H3	Cell Signaling	5192
Rho-GDI	Cell Signaling	2564
HSC70	B-6	7298
Donkey anti-goat IgG-HRP	Promega	V805A
goat anti-rabbit IgG-HRP	Invitrogen	65–6120
goat anti-mouse IgG-HRP	Invitrogen	62–6520
Ki67	Cell Signaling	9027
Biotin conjugated goat anti-rabbit IgG	Invitrogen	31820
Cleaved Caspase-3	Cell Signaling	9579
p-AKT (S473)	Cell Signaling	3787
VAMP2	Cell Signaling	13508
P-CXCR2	Thermo Fisher Scientific	PA5–104850
B3-tubulin	Cell Signaling	5568
Alexa Fluor 647 donkey anti-rabbit	Thermo Fisher	A31573
Alexa Fluor 488 goat anti-rabbit	Thermo Fisher	A11008
Fluorescin Phalloidin	Thermo Fisher	F432
WGA Alexa Fluor 647 Conjugate	Thermo Fisher	W32466
SUMO1	Cell Signaling	4930
Other		
TP53 shRNA	Open BioSystems Inc Corporation	V3LHS_333919 V3LHS_333920 V3LHS_404717
RB1 shRNA	Open BioSystems Inc Corporation	V2LHS_130606 V2LHS_340824 V2LHS_340827
NRP2 siRNA	Dharmacon RNA Technologies	L-017721–00–0010 J-017721–06–0005 J-017721–07–0005 J-017721–08–0005 J-017721–09–0005
VAMP2 siRNA	Dharmacon RNA Technologies	L-012498–00–0005

REAGENT or RESOURCE	SOURCE	IDENTIFIER
Non targeted control	Dharmacon RNA Technologies	LU-017721–00–005
Bacterial and virus strains		
Top10	Thermo Fisher Scientific	C404003
Experimental models: Cell lines		
C4–2	ATCC and gift from Prof. Allen Gao	CRL-3314
C4–2B	ATCC and gift from Prof. Allen Gao	CRL-3315
HEK293T	ATCC	CRL-3216
NCI-H660	ATCC	CRL-5813
Critical commercial assays		
cDNA kit	Roche	04379012001
Proteome profiler array (Human XL cytokine Array kit	R&D Systems	ARY022B
Vybrant Apoptosis Assay Kit	Molecular Probes (Invitrogen)	V13243
MTT assay	Cayman Chemical	10009365
Other reagents		
Reagent A: Avidin	Thermo Scientific	1852280
Reagent B: Biotinylated HRP	Thermo Scientific	1852310
ImmPACT DAB	Vector Laboratories	SK-4105
Recombinant human IL-8	R&D Systems	208-IL
Recombinant VEGFC	R&D Systems	9199-VC-025
Halt phosphatase inhibitor	ThermoFisher Scientific	1862495
TRIzol Reagent	ThermoFisher Scientific	15596018
PowerSYBR Green master mix	ThermoFisher Scientific	4367659
Enzalutamide	Sellekchem	S1250
Docetaxel	Mylan	NDC 67457–531–02
Doxycycline hyclate	Sigma-Aldrich	D9891–5G
Ketamine hydrochloride	Zoetis	NADA #043–304
Xylazine	Patterson Veterinary	NDC 14043–700–50
Cisplatin	Teva Generics	NDC 0703–5747–11
Etoposide	Abcam	ab120227
Gibco RPMI 1640	ThermoFisher Scientific	11875–093
FBS	Sigma-Aldrich	F2442
BSA	Sigma-Aldrich	A7906–500G
DPBS	Corning	21–031-CV
Trypsin	ThermoFisher Scientific	25200–056
TransIT-X2 Transfection Reagent	Dharmacon RNA Technologies	T-2005–02
precast 4–20% Mini-PROTEAN® TGX™ Gel	BioRad	4561094
PVDF membrane	BioRad	1620184
SuperSignal™ West Femto Maximum Sensitivity Substrate	ThermoFisher Scientific	34095
SuperSignal™ Pico Maximum Sensitivity Substrate	ThermoFisher Scientific	
Dako antigen retrieval solution (pH6)	Agilent Technologies	S1700